Journal of Medical and Biological Engineering (2018) 38:993–1013
https://doi.org/10.1007/s40846-018-0386-x

ORIGINAL ARTICLE

Computational Design of an RF Controlled Theranostic Model for Evaluation of Tissue Biothermal Response

Bamidele Omotayo Awojoyogbe[1,2] · Michael Oluwaseun Dada[1]

Received: 20 January 2017 / Accepted: 13 December 2017 / Published online: 17 March 2018

Abstract

Human disease management strategies are gradually shifting from the traditional approach towards personalized medicine. Thermal therapy comprising of clinical hyperthermia and therapeutic hypothermia has been subject of recent research. However, both have suffered in clinical trials because thermal monitoring is not impressive and delivering the appropriate amount of heat to the appropriate part of the patient's tissues is challenging. Hence, this study is aimed at addressing these challenges by technically merging the principles of magnetic resonance relaxation to the Bioheat transfer phenomenon. The analytical solutions to the Pennes Bioheat equation are connected to radiofrequency (RF) power absorption in tissue that is dependent on the magnetic resonance relaxation parameters. A carefully selected RF field is used to control the model for hyperthermia and therapeutic hypothermia. The solution obtained is then applied to hyperthermia treatment of tumours and therapeutic hypothermia of the brain. The thermal profiles obtained do not only show excellent contrasts between different tissues but real time monitoring of tissue thermal response is very impressive. By producing individualized virtual tumours that may predict disease progression, the thermal profiles based on the controlled parameters developed in this study can contribute to the ongoing dialogue regarding the design of appropriate response criteria, provide a means to perform virtual clinical trials to assess the likely benefit of novel neurotherapeutics, and move neuro-oncology toward individualized treatment plans optimized for maximum benefit.

Keywords Magnetic resonance imaging · Bioheat equation · Theranostics · Specific absorption rate (SAR) · Hyperthermia · Therapeutic hypothermia

List of symbols

ρ	Tissue density (kgm^{-3})
c	Specific heat of tissue ($Jkg^{-1}K^{-1}$)
T	Tissue temperature (^0C)
t	Exposure time (s)
W_0	Volumetric perfusion rate ($kgm^{-3}s^{-1}$)
c_b	Specific heat of blood ($Jkg^{-1}K^{-1}$)
ρ_b	Density of blood (kgm^{-3})
T_b	Supplying arterial blood temperature (^0C)
k	Thermal conductivity of tissue ($Wm^{-1}K^{-1}$)
SAR	The local specific absorption rate (Wm^{-3})
γ	Gyromagnetic ratio ($s^{-1}T^{-1}$)
M_0	Equilibrium magnetization (Am^{-1})
ω	Irradiation frequency of the RF field (Hz)
ω_o	Larmor frequency corresponding to the static field (Hz)
ω_1	Frequency of RF-induced rotation (Hz)
T_1	Transverse relaxation time (s)
T_2	Longitudinal relaxation time (s)
α	Thermal diffusivity (m^2s^{-1})
Q_0	A constant temperature (^0C)
P_{rf}	RF power absorbed per unit volume by the spins of the tissues
B_1	RF magnetic field (T)
B_0	Static magnetic field (T)
G	Magnetic field gradient (Tm^{-1})
ξ	RF dimensionless controlled parameter
T_m	Assumed constant initial temperature for controlled localized hyperthermia (^0C)
f(x)	Spatially dependent temperature just before the application of RF field (^0C)

✉ Bamidele Omotayo Awojoyogbe
abamidele@futminna.edu.ng; awojoyogbe@yahoo.com

[1] Department of Physics, Federal University of Technology, PMB 65, Minna, Niger State, Nigeria

[2] Department of Physics, University of Ilorin, PMB 1515, Ilorin, Kwara State, Nigeria

1 Introduction

Recently, the cost of disease diagnosis and treatment has been on the rise [1]. Unfortunately, the rising cost is not translating to significant reduction in disease related deaths. Recent disease management strategies are now gradually shifting from the traditional "one drug fits all" approach towards personalized medicine, in which drugs are specifically administered to a patient at the right time [1–3]. Although the possibilities and prospects of personalized medicine are undoubtedly impressive, its potential is yet to be fully explored [1, 4, 5]. In recent times, it has been discovered that heterogeneous diseases may be attacked effectively by developing specific treatment plans that are generally referred to as personalized treatments or theranostics [6].

Theranostics is a portmanteau of therapeutics and diagnostics. It can be diagnosis followed by therapy to stratify patients who will likely respond to a given treatment or therapy followed by diagnosis to monitor early response to treatment and predict treatment efficacy. It is also possible that diagnostics and therapeutics are developed together [7]. The utmost goal of theranostics is to gain the ability to image and monitor the diseased tissue, delivery kinetics, and drug efficacy with the long-term hope of gaining the ability to tune the therapy and drug dose with ultimate control [8, 9]. It has also helped in streamlining the drug discovery and development processes due to the number of scientific breakthroughs that have been brought together in the course of developing theranostic modalities [1]. For example, the human genome project and the development of biomarker initiatives have led to improved understanding of human disease progression [1, 10]. Theranostic methods avail clinical scientists and physicians with high value scientific decision-making during treatment of diseases. It has the ability to identify patients who may not respond to a drug or who are likely to experience side effects thereby improving clinical outcomes and safety [1, 10]. Theranostics has proved to be very important in increasing the efficiency of drug development processes by elucidating mapping of patients to the benefits of new drugs; thus improving health economic planning since physicians now have more control over the choice of optimal and cost effective therapy to be employed [10].

There is obviously no doubt in the potential of theranostics in improving healthcare. However, there are a number of challenges that must be overcome before becoming exclusively embedded in routine clinical practices [1, 10]. One of the most important challenges is the availability and use of a single platform for diagnosis and therapy.

Several theranostics strategies have been developed for the diagnosis and treatment of human diseases, mostly with emphasis on imaging and treatment of cancer [8]. For example, therapeutic modalities such as nucleic acid delivery, chemotherapy, hyperthermia (photo-thermal ablation), photodynamic, and radiation therapy are presently being combined with one or more imaging functionalities for both in vitro and in vivo studies of diseases [8]. In fact, several imaging agents, such as magnetic resonance imaging (MRI) contrast agents (T_1 and T_2 agents) [8, 11], fluorescent markers [8, 12] (organic dyes and inorganic quantum dots), and nuclear imaging agents (PET/SPECT agents), can be functionalized with therapeutic agents or therapeutic delivery methods [12] in order to facilitate their imaging and consequently gain information about the trafficking pathway, kinetics of delivery and therapeutic efficacy [8]. New theranostics methods using MRI and boron capture therapy (BNCT) for treatment of cancer are now widely explored [13, 14].

It has recently been suggested that it is possible to develop a dedicated theranostic methods in which a specially selected RF field is used to heat up tissues and simultaneously cause the spins of the tissue to emit magnetic resonance signals [15]. This method may also be termed thermal therapy [16] which comprises of hyperthermia treatment (commonly called clinical hyperthermia) [17, 18] and therapeutic hypothermia [19].

Therapeutic hypothermia is a clinical treatment technique which is used to decrease the body core temperature and according to recent research efforts [20–22], target temperature ranges between 32 and 34 °C have been suggested for use in post-cardiac arrest therapeutic scenarios. This is consistent with clinical recommendations. For example, physiological problems that cause circulatory arrest within the brain leads to a sequence of neurological events; consciousness is lost within the first 10 s and after 20 s, electroencephalographic activity shows no net electrical charge [21, 23]. As a consequence, energy stores become depleted due to anaerobic glycolysis [20]. Along with energy depletion, there exists cellular depolarization in which normal calcium ion balance between intracellular and extracellular compartments is completely violated [20, 23]. This violation results in accumulation of calcium in the inner compartment of the cells and eventually leads to premature neuronal death [22, 24].

Even after the restoration of blood flow to the tissues, the activation of N-methyl-D-aspartate (NMDA) receptors could lead to increase in body temperature above 37 °C with further increase in intracellular calcium levels and more neuron deaths [20, 25]. In this case, therapeutic hypothermia becomes useful because its ability of reducing cerebral metabolic rate becomes temperature-dependent. The protective capability of therapeutic hypothermia is achieved through the reduction of the oxygen consumption, glucose utilization and lactate concentration [20].

It is worth noticing that an ideal portable cooling device which has the ability to achieve quick temperature reductions, has preferential organ cooling capability and could be implemented on multi-setting clinical platforms is presently unavailable [20, 26]. This is the reason why hypothermia methods making use of personalized medicine could become important for treating emergency cases.

State-of-the-art methods of therapeutic hypothermia are classified into noninvasive (surface) techniques and invasive techniques. Noninvasive techniques include hydrogel-coated cooling pads, immersion in cold water, cooling helmets (caps), ice packs and cooling blankets. Invasive techniques include infusion of cold intravenous fluids, intra-ventricular cerebral hypothermia, extracorporeal circulating cooled blood, retrograde jugular vein flush, peritoneal lavage with cold exchanges, nasopharyngeal balloon catheters and nasal, nasogastric (and rectal) lavage [20]. Noninvasive methods are mostly used for hypothermia treatment because their implementation is not difficult but the attainment of desired body temperature takes a relatively long time (between 2 and 8 h). In additional to this downside, they are unable to penetrate to deep organs such as the brain and the heart. The requirement of this method also leads to exaggerated shivering response [20, 27, 28]. Furthermore, temperature monitoring and feedback with surface methods are extremely difficult. Clinical methods that are able to address this problem are expensive but desirable. An example of a higher cost methods is the use of hydrogel-coated pads in which temperature-controlled water is circulated under negative pressure, which has been able to achieve an average temperature reduction rate of 1.4 °C per hour, while the target temperature was achieved in less than 2.5 h [29]. Despite the improvements made with this higher cost methods, the time to realize the target temperature is still large enough to constitute heat loads on the tissues [30]. Although invasive methods have proved to be significant improvements over surface methods, they are currently cumbersome, require extremely clean surroundings and limited to the in-hospital environment [20]. Research efforts to address these challenges are currently being tilted towards the development of non-invasive and invasive methods for selective brain cooling, especially for emergency cases.

Therapeutic hypothermia has been a subject of great interest for neuroprotection in traumatic brain injury (TBI) [31] but cooling the injured brain to limit TBI damage has not been promising for TBI treatment according to clinical trials [20]. Some of these problems could be centred on faults in the design of clinical trials or in the insufficiency of a single agent to prevent the array of injury processes involved in secondary injury [31]. A theranostics therapeutic hypothermia treatment in which the tissue cooling process may be mapped in real time could possibly mitigate the problems that have been highlighted above.

Hyperthermia may be regarded as raising the temperature of a part of or the whole body above normal levels for a defined period. The extent of temperature elevation associated with hyperthermia is about a few degrees above normal temperature (41–45 °C) [17]. State-of-the-art methods in hyperthermia can be classified based on tumour location, tumour depth and tumour staging. They are local hyperthermia (useful for superficial, intracavital, intraluminal and intracranial tumours), regional hyperthermia (useful for deep seated and locally advanced tumours) and whole body hyperthermia (useful for disseminated/metastatic diseases) [32]. Thermal energies are delivered via microwave, radiofrequency (100 kHz–150 MHz), infrared radiators, resistive wire implants, ferromagnetic seeds, magnetic nanoparticles, ultrasound and hot water perfusion [32, 33].

Local hyperthermia is particularly suited to small tumours (with diameters between 3 cm and 6 cm) and mostly makes use of microwaves, radio waves or ultrasound for heat delivery [33, 34]. Side effects are prevented with the use of water bolus for cooling and maintenance of skin temperature at about 37 °C. With this technique, interstitial heating is possible with the use of radiofrequency ablation in which the temperature of the target tissue is increased to over 50 °C for more than 4–6 min (more than 512 cumulative equivalent minutes (CEM) 43 °C) [32, 35].

Regional hyperthermia is suitable for thermal treatment of large body parts such as the abdominal cavity (especially organs and limbs). This method is generally employed in the treatment of advanced tumours such as cervical, bladder, prostate, soft tissue sarcomas, colorectal and ovarian carcinomas. The approaches used in the implementation of this thermal treatment method are the use of applicators for deep-seated tumours, thermal perfusion for limbs/organs and continuous hyperthermic peritoneal perfusion. External applicators, which consist of coherent arrays of dipole antenna pairs, are sometimes used to treat these tumours. They emit microwave or radiofrequency energy to specifically target metastatic parts of the body. These applicators have the ability of raising the temperature of the targeted body regions to between 41 and 42 °C but limited by power deposition (specific absorption rate—SAR) in surrounding tissues [32, 33]. However, proper planning and treatment monitoring with this method has been challenging and recently, magnetic resonance tomography is being explored for non-invasive recording of tissue temperatures and perfusion in deep regional hyperthermia [36].

Whole-body hyperthermia is well suited to patients with disseminated tumours such as soft tissue sarcoma, melanoma and ovarian cancer. It gives the most homogeneous thermal distribution while subjecting patients to general anaesthesia for extreme whole-body hyperthermia (about 42.0 °C for 1 h) or deep sedation for moderate whole-body hyperthermia (39.5–41.0 °C for 3–4 h) [32]. However, this

method has been associated with a high risk of complications such as thermal stress to the heart, liver, lungs or brain. Other problems such as nausea, vomiting and transient diarrhoea have been recorded during whole-body hyperthermia treatment [33, 37].

Local hyperthermia has demonstrated to be very effective when combined with chemotherapy or radiation therapy for cancers such as breast, cervical, prostate, head and neck, melanoma, soft tissue sarcoma and rectal cancers etc. [38]. Whole body hyperthermia is generally considered a promising experimental cancer treatment but requires close medical monitoring of the patient because of associated side effects [38]. This problem echoes the challenges in thermal therapy, which is delivering the appropriate amount of heat to the appropriate part of the patient's tissues [39–41]. For example, an effective thermal therapy procedure may require tissue temperatures to be raised and sustained long enough in order for cancer cells to be incapacitated or killed. However, if the temperatures are too high or sustained for times for which the tissue cells are unable to handle, serious side effects, including death may occur. Hence, the smaller the size of the heated tissue region and the shorter the thermal treatment time, the lower the side effects [39–41]. Unfortunately, tumour treated at extremely low temperatures and for short periods of time will not achieve therapeutic goals. Therefore, since all methods of inducing higher temperatures in the body are countered by the thermoregulatory mechanisms of the body, it is of utmost importance that new thermal therapy methods that are sensitive to the human thermoregulatory mechanisms, will be developed. This is the focus of this study and we intend addressing the problem by technically merging magnetic resonance relaxation mechanism with the Bioheat transfer phenomenon. Fortunately, the proposed solution will address the safety related challenge in MRI examinations because traditionally, the transmission of radiofrequency (RF) excitation pulses gives rise to temperature elevation in the various tissues and organs of the patient's body [42]. Therefore, in addition to theranostics features of the proposed method, we can also achieve body temperature monitoring and control during magnetic resonance examinations.

Section 2 derives a mathematical method, which utilizes the principles of magnetic resonance relaxation for the bio-heat transfer phenomenon. An analytical solution to the Pennes bio-heat equation is connected to radio frequency power absorption in tissues. The solution is applied to hyperthermia treatment of tumour and therapeutic hypothermia of the brain. Section 3 clearly illustrates the advantages and application of Pennes bio-heat equation and nuclear magnetic resonance (NMR) relaxation parameters such that it is possible to perform hyperthermia treatment of tumours and monitor temperature changes without heating up surrounding normal tissues. This section also demonstrates how the theranostics approach is able to provide real time monitoring of tissues during hyperthermia treatment of tumours with impressive thermal energy deposition control. The performance benefits of the proposed system are demonstrated through simulations. Section 4 discusses the thermal therapy comprising of clinical hyperthermia and therapeutic hypothermia with focus on addressing those challenges that limits the clinical application of current hyperthermia methods combined with conventional treatment modalities such as ionizing radiation and chemotherapy by technically merging the principles of magnetic resonance relaxation to the bio-heat transfer phenomenon. Analytical solutions to Pennes bio-heat equation connecting to power absorption of RF in tissue which is dependent on the magnetic resonance relaxation parameters, are presented. Section 5 gives specific advantages of the proposed magnetic resonance-based theranostic model suitable for imaging tissue responses during hyperthermia treatment of tumours and therapeutic hypothermia of brain tissues over current hyperthermia combined with conventional treatment modalities.

2 Method

Since changes in temperature in various organs and tissues of the body during a magnetic resonance imaging procedure are hitherto difficult to measure in clinical routine [42], radiofrequency (RF) exposure of patients is usually characterized by means of the specific absorption rate (SAR). Meanwhile, the temperature rise in localized tissue regions is not only dependent on the localized SAR and the duration of the MR sequence applied, but also on thermal conductivity and micro vascular blood flow leading to thermal equilibrium within the body [42]. For assessing micro vascular heat transfer in biological tissues, different continuum models have been proposed in the form of a modified heat diffusion equation in which the effects of micro vascular blood flow were properly considered. However, continuum approaches often neglects the local effects of "thermally significant" blood vessels entering the heated region. Hence, heat transfer analysis often requires simultaneous consideration of transient and spatial heating inside biological systems [43]. The Pennes bio-heat transfer equation, which describes the exchange of heat between tissue and blood [42, 43], is widely used to monitor the temperature distribution in various tissues for thermal therapy [43–48]. This distribution can be defined mathematically based on the Pennes's bio-heat equation in the presence of a source of RF heating as follows [15, 42]:

$$\rho c\frac{\partial T}{\partial t} = \nabla(k\nabla T) + \rho SAR - W_0\rho_b c_b(T - T_b) \tag{1}$$

where ρ is tissue density, ρ_b is density of blood, c is specific heat of tissue, T is tissue temperature, t is exposure time, W_0 is volumetric perfusion rate, c_b is specific heat of blood, T_b

is supplying arterial blood temperature, k is thermal conductivity of tissue and SAR is local specific absorption rate.

Considering the transient problem involving the bio-heat equation within a small voxel of human tissue, a one-dimensional problem in which the parameter x is the depth in tissue from a reference point on the tissue surface could be written from Eq. (1) as follows:

$$\rho c\frac{\partial T}{\partial t} = k\frac{\partial^2 T}{\partial x^2} + \rho SAR - W_0\rho_b c_b(T - T_b) \tag{2}$$

In order to solve Eq. (1), SAR is defined as:

$$SAR = \frac{W_0\rho_b c_b Q_0}{\rho} = \frac{\beta_b Q_0}{\rho} \tag{3}$$

where Q_0 is a constant (which has the unit of temperature). Equation (2) may then be written as [26]:

$$\rho c\frac{\partial T}{\partial t} = k\frac{\partial^2 T}{\partial x^2} - \beta_b\theta \tag{4}$$

where

$$\theta = T - T_b - Q_0 \tag{5}$$

Equation (4) then becomes:

$$\rho c\frac{\partial \theta}{\partial t} = k\frac{\partial^2 \theta}{\partial x^2} - \beta_b\theta \tag{6}$$

By the method of separation of variables, we can write [49]:

$$\theta(x,t) = X(x)\Omega(t) \tag{7}$$

where X(x) is the spatially dependent variable while Ω(t) is the time dependent variable. Equation (6) then becomes:

$$\rho cX\frac{d\Omega}{dt} = k\Omega\frac{d^2X}{dx^2} - \beta_b X\Omega \tag{8}$$

If we multiply both sides of Eq. (8) by $\frac{1}{k\Omega X}$, we obtain:

$$\frac{\rho c}{k\Omega}\frac{d\Omega}{dt} + \frac{\beta_b}{k} = \frac{1}{X}\frac{d^2X}{dx^2} \tag{9}$$

By the principle of separation of variables, Eq. (9) must be equal to a constant [49] $-\lambda^2$($-\lambda^2$ is a fundamental constant of separation of variables. X(x) and Ω(t) are used for standard evaluation of Bessel integral equation) and gives the following equations:

$$\frac{d\Omega}{dt} = -\frac{k}{\rho c}\left(\frac{\beta_b}{k} + \lambda^2\right)\Omega \tag{10}$$

$$\frac{d^2X}{dx^2} = -\lambda^2 X \tag{11}$$

The solutions to Eqs. (10) and (11) are:

$$\Omega(t) = A_0 e^{-\alpha\left(\frac{\beta_b}{k}+\lambda^2\right)t} \tag{12}$$

$$X(x) = P_1\cos\lambda x + P_2\sin\lambda x \tag{13}$$

According to Eqs. (7), (12) and (13) we write:

$$\theta(x,t) = e^{-\alpha\left(\frac{\beta_b}{k}+\lambda^2\right)t}(A_1\cos\lambda x + A_2\sin\lambda x) \tag{14}$$

where $\alpha = \frac{k}{\rho c}$ is the thermal diffusivity and $A_1 = A_0P_1$, $A_2 = A_0P_2$.

We shall make use of initial boundary conditions that are realistic in bio-heat transfer for human tissues. If at the point x = 0, the contribution to the measured temperature is only from the arterial blood flow, we write:

$$T(x,t)|_{x=0} = T_b + Q_0 \tag{15}$$

Hence, from Eq. (15),

$$\theta(x,t)|_{x=0} = 0 \tag{16}$$

Similarly, if at t = 0, the contributions to the measured temperature are captured by the equation:

$$T(x,t)|_{t=0} = f(x) + T_b + Q_0 \tag{17}$$

where f(x) is a spatially dependent temperature just before the application of RF field. Equation (17) implies that

$$\theta(x,t)|_{t=0} = f(x) \tag{18}$$

Using the condition in Eq. (16), $A_1 = 0$, Eq. (14) becomes:

$$\theta(x,t) = A_2 e^{-\alpha\left(\frac{\beta_b}{k}+\lambda^2\right)t}\sin\lambda x \tag{19}$$

It is possible to replace the constant P_2 by a function $P_2(\lambda)$ and still have a solution [49–52]. Furthermore, we can integrate this function over λ from 0 to ∞. This is similar to the superposition theorem for discrete values of λ used in connection with Fourier series. Consequently, a possible solution to Eq. (6) is:

$$\theta(x,t) = \int_0^\infty A_2(\lambda)e^{-\alpha\left(\frac{\beta_b}{k}+\lambda^2\right)t}\sin\lambda x d\lambda \tag{20}$$

From Eqs. (18) and (20), we obtain:

$$f(x) = \int_0^\infty A_2(\lambda)\sinh\lambda x d\lambda \tag{21}$$

The representation in Eq. (21) implies that $f(x)$ must be an odd function [49] and hence,

$$A_2(\lambda) = \frac{2}{\pi}\int_0^\infty f(u)\sin\lambda u du \tag{22}$$

If we use this expression in Eq. (20), we write:

$$\theta(x,t)=\frac{2}{\pi}\int_0^\infty\int_0^\infty f(u)e^{-\alpha\left(\frac{\beta_b}{k}+\lambda^2\right)t}\sin\lambda u\sin\lambda x d\lambda du \tag{23}$$

The results in Eq. (23) could be written as:

$$\theta(x,t)=\frac{1}{\pi}\int_0^\infty\int_0^\infty f(u)e^{-\alpha\left(\frac{\beta_b}{k}+\lambda^2\right)t}[\cos\lambda(u-x)-\cos\lambda(u+x)]d\lambda du \tag{24}$$

$$\theta(x,t)=\frac{1}{\pi}\int_0^\infty f(v)\left\{\int_0^\infty e^{-\alpha\left(\frac{\beta_b}{k}+\lambda^2\right)t}\cos\lambda(u-x)d\lambda-\int_0^\infty e^{-\alpha\left(\frac{\beta_b}{k}+\lambda^2\right)t}\cos\lambda(u+x)d\lambda\right\}dv \tag{25}$$

$$\theta(x,t)=\frac{1}{\pi}\int_0^\infty f(v)e^{-\frac{\alpha\beta_b}{k}t}\left\{\int_0^\infty e^{-\alpha\lambda^2t}\cos\lambda(u-x)d\lambda-\int_0^\infty e^{-\alpha\lambda^2t}\cos\lambda(u+x)d\lambda\right\}dv \tag{26}$$

However, the integrals in Eq. (25) could be resolved into [49]:

$$\int_0^\infty e^{-a\lambda^2}\cos b\lambda d\lambda=\frac{1}{2}\sqrt{\frac{\pi}{a}}e^{-\frac{b^2}{4a}} \tag{27}$$

Therefore, Eq. (26) becomes:

$$\theta(x,t)=\frac{1}{2\sqrt{\pi\alpha t}}e^{-\frac{\alpha\beta_b}{k}t}\left[\int_0^\infty f(u)e^{-\frac{(u-x)^2}{4\alpha t}}du-\int_0^\infty f(u)e^{-\frac{(u+x)^2}{4\alpha t}}du\right] \tag{28}$$

Setting $\frac{(u-x)}{2\sqrt{\alpha t}}=\varepsilon$ in the first integral and $\frac{(u+x)}{2\sqrt{\alpha t}}=\varepsilon$ in the second integral; $du=2\sqrt{\alpha t}d\varepsilon$, then Eq. (28) becomes:

$$\theta(x,t)=\frac{1}{\sqrt{\pi}}e^{-\frac{\alpha\beta_b}{k}t}\left[\int_{\frac{-x}{2\sqrt{\alpha t}}}^\infty e^{-\varepsilon^2}f(2\varepsilon\sqrt{\alpha t}+x)d\varepsilon-\int_{\frac{x}{2\sqrt{\alpha t}}}^\infty f(2\varepsilon\sqrt{\alpha t}-x)e^{-\varepsilon^2}d\varepsilon\right] \tag{29}$$

The temperature f(x) would be taken to be the tissue metabolic heat contribution to the measured temperature. If we assume a constant initial temperature such that $f(x)=T_m$, we obtain

$$\theta(x,t)=\frac{T_m}{\sqrt{\pi}}e^{-\frac{\alpha\beta_b}{k}t}\sqrt{\pi}erf\left(\frac{x}{2\sqrt{\alpha t}}\right)=T_me^{-\frac{\alpha\beta_b}{k}t}erf\left(\frac{x}{2\sqrt{\alpha t}}\right) \tag{30}$$

Equations (5), (7) and (30) give,

$$T(x,t)=T_b+Q_0+T_me^{-\frac{\alpha\beta_b}{k}t}erf\left(\frac{x}{2\sqrt{\alpha t}}\right) \tag{31}$$

$$T(x,t)=T_b+\frac{\rho SAR}{W_0\rho_bc_b}+T_me^{-\frac{\alpha\beta_b}{k}t}erf\left(\frac{x}{2\sqrt{\alpha t}}\right) \tag{32}$$

In order to introduce the diagnostic part of the model, it is important to note that the RF power absorbed per unit volume by the spins of the tissues being investigated (including tumour) is given as [53]:

$$\frac{P_{rf}}{V}=-\frac{\omega\gamma B_1^2T_2}{1+(\Delta\omega)^2T_2^2+\gamma^2B_1^2T_1T_2}M_0 \tag{33}$$

where ω is irradiation frequency of the RF field, $\omega_o=\gamma B_0$ is Larmor frequency corresponding to the static field, $\omega_1=\gamma B_1$ is frequency of RF-induced rotation, $\Delta\omega=\omega-\omega_0$, γ is gyromagnetic ratio, T_2 is transverse relaxation time, T_1 is longitudinal relaxation and M_0 is equilibrium magnetization [53–57].

Specific absorption rate (SAR) is a measure of the rate at which energy is absorbed by the human body when exposed to RF electromagnetic field [54, 55]. It is defined as the power absorbed per mass of tissue and expressed as follows [55]:

$$SAR=\frac{P_{rf}}{m}=\frac{P_{rf}}{\rho V} \tag{34}$$

where m is the mass of the tissue, V the tissue volume and ρ the tissue density. From Eqs. (33) and (34), we obtained:

$$\rho SAR = -\frac{\omega\gamma B_1^2 T_2 M_0}{1+(\omega-\omega_0)^2T_2^2+\gamma^2B_1^2T_1T_2} \tag{35}$$

Finally, from Eq. (32), we have:

$$T(x,t) = T_b - \left(\frac{\omega\gamma B_1^2 T_2}{W_0\rho_b c_b}\right)\frac{M_0}{1+(\omega-\omega_0)^2T_2^2+\gamma^2B_1^2T_1T_2} + T_m e^{-\frac{\alpha\beta_b}{k}t} erf\left(\frac{x}{2\sqrt{\alpha t}}\right) \tag{36}$$

It should be noted that the solution obtained in Eq. (36) is not rigid but strictly dependent on the prevailing NMR condition based on the following conditions [56, 57]:

(i) Adiabatic condition holds when $\gamma^2B_1^2T_1T_2 >> 1$,

$$T(x,t) = T_b - \left(\frac{\omega\gamma B_1^2 T_2}{W_0\rho_b c_b}\right)\frac{M_0}{1+(\omega-\omega_0)^2T_2^2+\gamma^2B_1^2T_1T_2} T_m e^{-\frac{\alpha\beta_b}{k}t} erf\left(\frac{x}{2\sqrt{\alpha t}}\right) \tag{37}$$

(ii) Non-adiabatic condition holds when $\gamma^2B_1^2T_1T_2 << 1$ (this is typically regarded as a linearity condition in which the frequency response takes on the characteristic Lorentzian form [58])

$$T(x,t) = T_b - \left(\frac{\omega\gamma B_1^2 T_2}{W_0\rho_b c_b}\right)\frac{M_0}{1+(\omega-\omega_0)^2T_2^2} + T_m e^{-\frac{\alpha\beta_b}{k}t} erf\left(\frac{x}{2\sqrt{\alpha t}}\right) \tag{38}$$

(iii) Saturation condition holds when $\gamma^2B_1^2T_1T_2 = 1$,

$$T(x,t) = T_b - \left(\frac{\omega\gamma B_1^2 T_2}{W_0\rho_b c_b}\right)\frac{M_0}{2+(\omega-\omega_0)^2T_2^2} + T_m e^{-\frac{\alpha\beta_b}{k}t} erf\left(\frac{x}{2\sqrt{\alpha t}}\right) \tag{39}$$

$$T(x,t) = T_b - \left(\frac{\omega\omega_1^2 T_2}{\gamma W_0\rho_b c_b}\right)\frac{M_0}{2+(\omega-\omega_0)^2T_2^2} + T_m e^{-\frac{\alpha\beta_b}{k}t} erf\left(\frac{x}{2\sqrt{\alpha t}}\right) \tag{40}$$

In the presence of magnetic field gradient, we may write [59–61]:

$$\omega_1 = \gamma B_1 = \gamma G\xi x \tag{41}$$

$$\omega - \omega_0 = \gamma G\xi x$$

where ξ is a dimensionless controlled parameter. For a system that presents non-adiabatic behaviour, we have:

$$T(x,t) = T_b - \left(\frac{\gamma^2G^2x^2(B_0+G\xi x)T_2}{W_0\rho_b c_b}\right)\frac{\xi^2M_0}{1+(\gamma G\xi x)^2T_2^2+T_1T_2(\gamma G\xi x)^2} + T_m e^{-\frac{\alpha\beta_b}{k}t} erf\left(\frac{x}{2\sqrt{\alpha t}}\right) \tag{42}$$

3 Analysis of Results

In this section, the mathematical results presented in Eq. (42) will be demonstrated in controlled thermal therapy. We will consider their theranostic applications in hyperthermia treatment (for tumour treatment) and therapeutic hypothermia (for neuroprotection treatment of the brain).

3.1 Theranostics of Tumours

Normal physiological temperature of human body is about 37.0 °C. Hyperthermia in which the temperature is between 42.0 and 46.0 °C has been shown to alter the function of many structural and enzymatic proteins within cells, which leads to necrosis [62]. In addition to necrotic cell death, hyperthermia may lead to decreases in cell growth and differentiation, and can also induce apoptosis and therefore, provide a treatment for tumour growth. In order to achieve controlled hyperthermia of tumours, we have proposed a theranostic method that provides thermal treatment of tumours in the presence of magnetic resonance tissue contrast. Tissue temperature as presented in Eq. (42) is used for tissue theranostics such that the second term on the right hand side of this equation provides both RF controlled thermal energy deposition as well as intra-tissue and inter-tissue MR contrasts. In addition, this expression provides a means of monitoring tissue temperature while assessing tissue state via T_1 and T_2 values in real time. We have calculated the temperature (presented in Table 1) based on Eq. (42) for several normal tissues and tumour assessed at magnetic field (B_0) of 1.5 T. The parameters used for these calculations are $G = 0.02 Tm^{-1}$ [63], $\gamma = 42666666.67\ s^{-1}T^{-1}$ [60], $T_b = 37.0$ °C [42], $T_m = 1.5$ °C, $M_0 = -500 Am^{-1}$, $\xi = 1$, $t = 3$ μs, $x = 5$ mm, $c_b = 3720 Jkg^{-1}K^{-1}$ [42], $\rho_b = 1060 kgm^{-3}$ [42]. It is noteworthy that we have set $T_0 = \frac{1}{T_1} + \frac{1}{T_2}$. The values of T_1 and T_2 used for the calculations were taken from [54].

The calculations were done by assuming that the non-adiabatic NMR condition holds within the system.

Thermal maps of normal and abnormal tissues after the application of RF energy was demonstrated by making three-dimensional plots of the tissue temperature distribution (using Sigma Plot 12—Systat Software, Inc) with reference to some selected parameters in Table 1. These plots or thermal maps have been presented in Figs. 1, 2 and 3. The maps were developed with consideration to different relaxation and thermal parameters according to the disease

Table 1 Calculation of tissue temperature from thermal properties and NMR relaxation parameters at 1.5T [42, 54, 59]

Tissue	ρ (kgm^{-3})	k ($Wm^{-1}K^{-1}$)	c ($Jkg^{-1}K^{-1}$)	W_0 ($kgm^{-3}s^{-1}$)	α (m^2s^{-1})	T_1(s)	T_2 (s)	T_0 (s^{-1})	T (°C)	SAR (Wm^{-3})
Skeletal muscle	1050	0.50	3465	0.0009	1.37×10^{-7}	1.030	0.060	17.63754	38.6939	0.655351
Kidney	1050	0.54	3700	0.061	1.39×10^{-7}	0.830	0.082	13.39994	38.50342	0.783260
Liver	1060	0.52	3600	0.015	1.36×10^{-7}	0.610	0.057	19.18320	38.51901	1.060860
Adipose tissue	950	0.27	3100	0.0005	9.17×10^{-8}	0.250	0.080	16.50000	39.65281	2.392499
Cortical bone	1920	0.79	1300	0.0013	3.17×10^{-7}	0.400	0.060	19.16667	38.81808	0.849240
Tumour	920	0.42	3000	0.000009	1.52×10^{-7}	0.926	0.120	9.413247	58.70538	0.779418

state of tissues. Table 1 and Figs. 1, 2 and 3 evaluate the tissue temperature at specific values of time of exposure and location (x). This implies that it is not possible to assess the temperature over varying time or location.

The use of Eq. (42) for thermal treatment and monitoring of abnormal tissues through MR contrasts may not be possible with the analyses presented above since the assessment of the tissue voxel is important and monitoring the effectiveness of delivered amount of thermal energy requires the variation of both time and space. In order to effectively address this challenge, we have developed a Wolfram Mathematica computer program for the assessment of the tissue thermal responses at varying voxel sizes and exposure times while making provisions for flexibility of changing any other important parameters for specific analyses. The thermal profiles obtained from this computer program are presented in Figs. 4, 5, 6, 7, 8 and 9. In these profiles, varying tissue dimensions (this is to take care of the suitability of the model for different sizes of proliferating tissues) and RF gradient fields (in order to investigate response of tissues to RF energy) were considered.

3.2 Therapeutic Hypothermia for Neuroprotection Treatment

It is known that therapeutic temperature regulation has become an interesting research field [64]. Mild-to-moderate hypothermia is a safe and feasible management modality for neuroprotection and control of intracranial pressure in neurological problems such as traumatic brain injury, subarachnoid and intracerebral hemorrhage and large hemispheric stroke. The efficacy of mild-to-moderate hypothermia has been demonstrated for neuroprotection after cardiac arrest with ventricular fibrillation as initial rhythm and after neonatal asphyxia [64]. Obviously, hypothermia has a bright future for cerebrovascular disease treatment if brain cooling can be delivered in a manner that does not compromise the patient or the neurosurgical and intensive care settings. Local brain

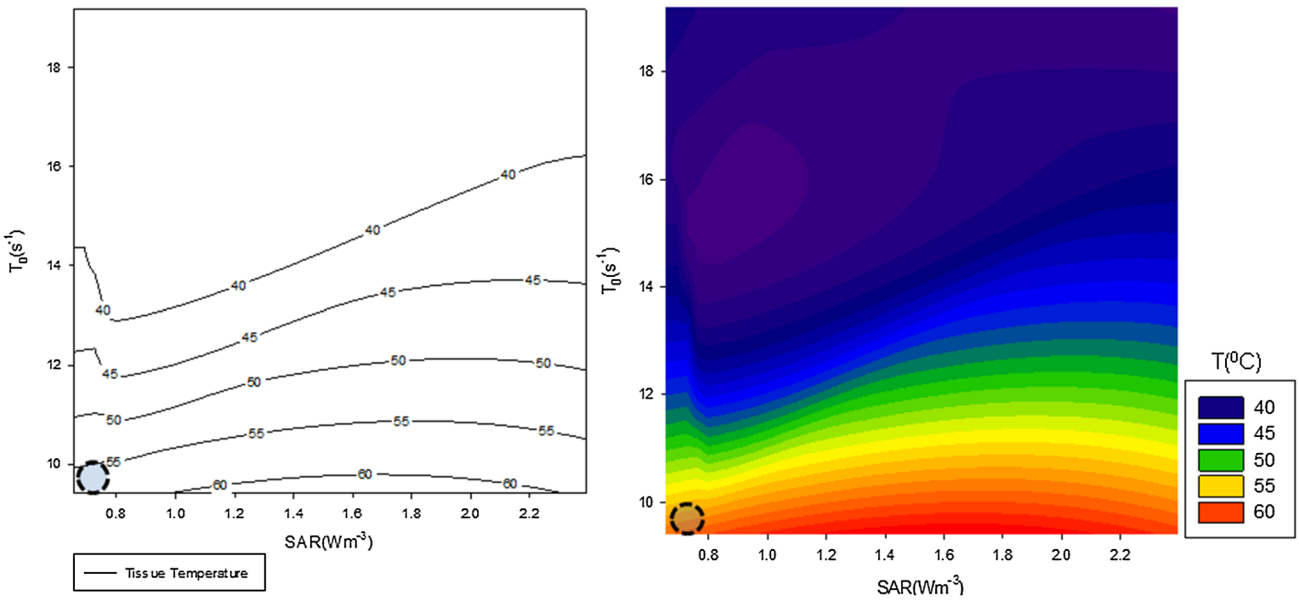

Fig. 1 Contour plots of the computed temperature as a function of relaxation rate, T_0 and SAR

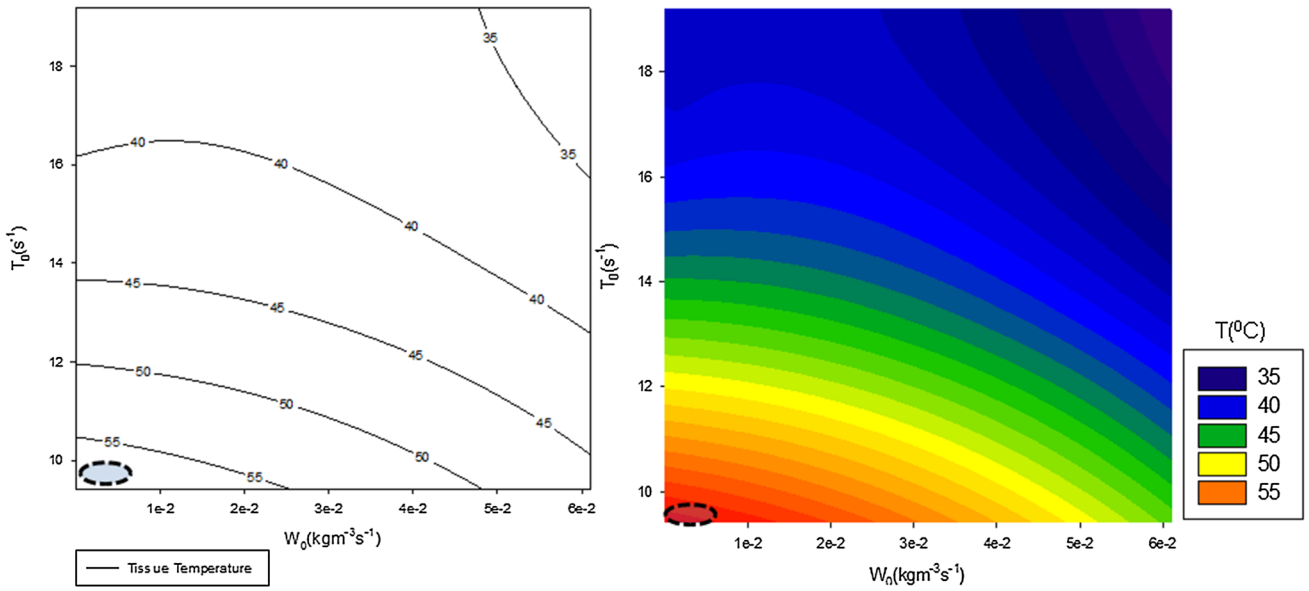

Fig. 2 Contour plots of the computed temperature as a function of relaxation rate, T_0 and volumetric perfusion rate, W_0

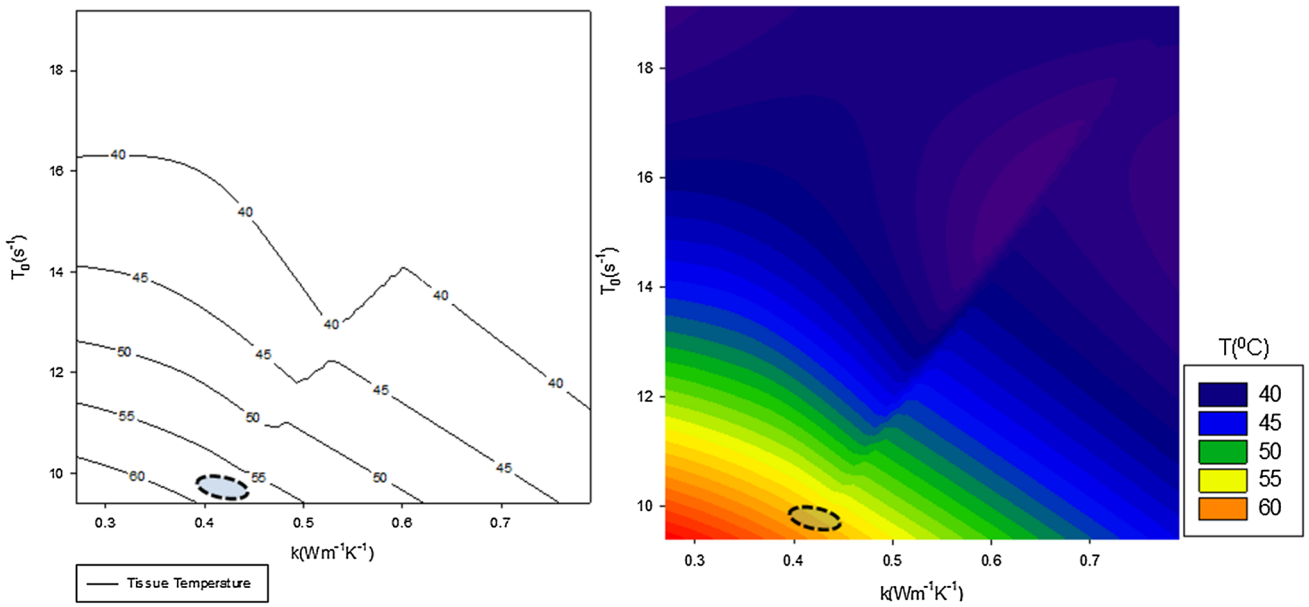

Fig. 3 Contour plots of the computed temperature as a function of relaxation rate, T_0 and thermal conductivity, k

cooling may be just that new treatment approach [65]. In this section, we present a tissue-specific hypothermia model based on the Pennes bio-heat equation. Fortunately, we do not have to seek new solutions to the bio-heat equation in order to address this problem. All that is needed to achieve hypothermia is to modify the behaviour of the parameter ξ such that the applied RF field is now complex [66]. In this case, for a Biothermal system showing non-adiabatic behaviour, we shall re-define the radio frequency as given in Eq. (41) as follows:

$$\omega_1 = \gamma B_1 = i\gamma G\xi x \tag{43}$$

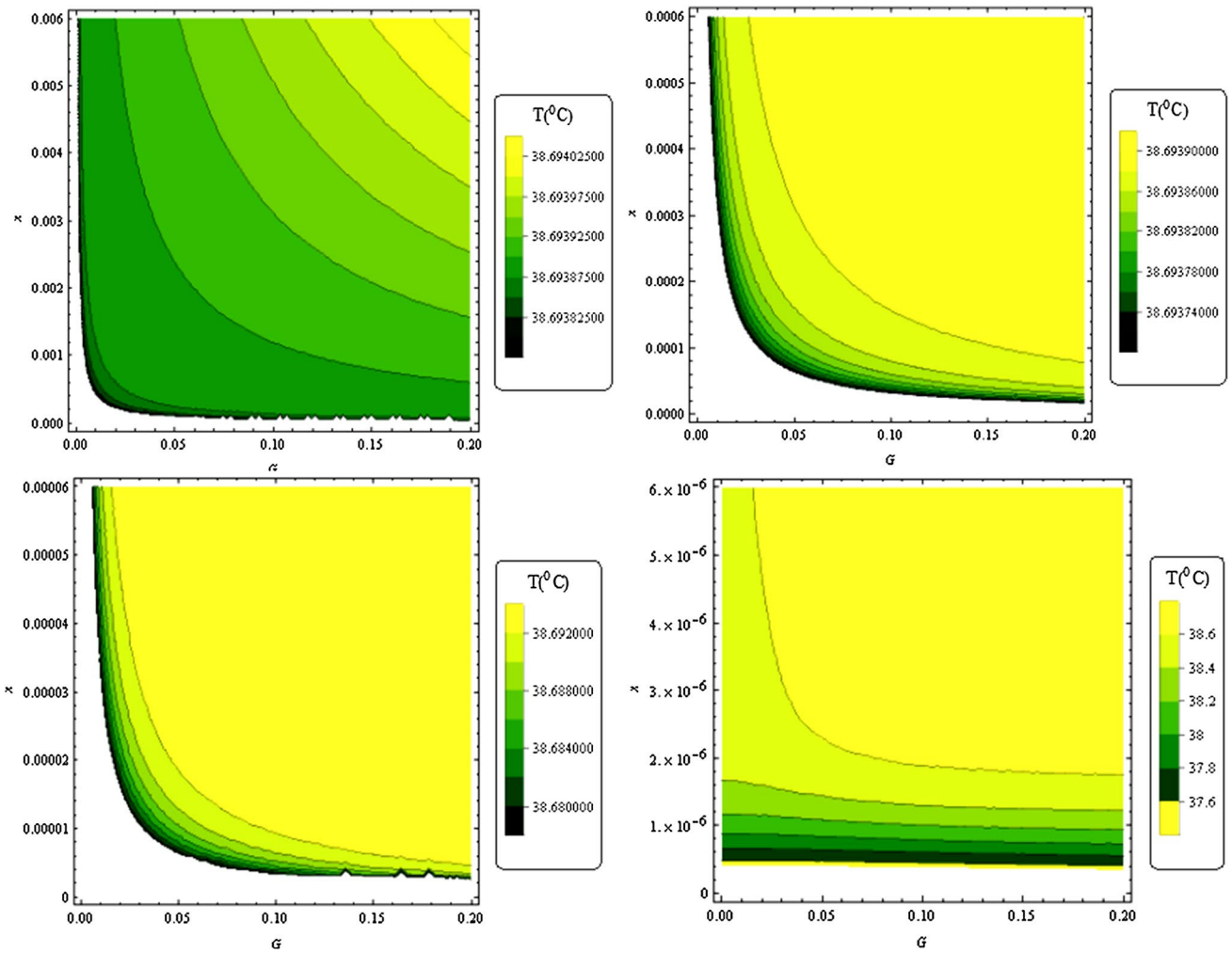

Fig. 4 Contour plots of the derived temperature as a function of the sampling point x and gradient pulse magnitude G for skeletal muscle at 1.5T

Hence, Eq. (42) becomes:

$$T(x,t) = T_b + \left(\frac{\gamma^2 G^2 x^2 (B_0 + |G\xi x|) T_2}{W_0 \rho_b c_b}\right) \frac{\xi^2 M_0}{1 - (\gamma G \xi x)^2 T_2^2 - T_1 T_2 (\gamma G \xi x)^2} + T_m e^{-\frac{\alpha \rho_b}{k} t} erf\left(\frac{x}{2\sqrt{\alpha t}}\right) \tag{44}$$

In order to obtain real values of tissue temperature, we have set the resultant magnetic field (in the rotating frame of reference) as:

$$\omega = B_0 + |B_1| = B_0 + |G\xi x| \tag{45}$$

Using Eqs. (43)–(45), we developed a Wolfram Mathematica computer program for creating thermal maps of *controlled* neuroprotection treatment of the human brain. To achieve this, we considered the treatment of the grey brain matter to be uniquely different from that of the white brain matter. The idea is that if the small biomolecular differences in these brain tissues show conspicuous differences on thermal maps, this method could prove to be good in treating delicate tissues like those of the brain. For the developed computer program, we assumed that the thermal features of the grey and white brain matter are not significantly different from those of the whole brain; hence, we used [54] $\rho = 1040 \text{kgm}^{-3}$, $c = 3640 \text{Jkg}^{-1}\text{K}^{-1}$, $k = 0.54\ \text{Wm}^{-1}\text{K}^{-1}$, $W_0 = 0.0073\ \text{kgm}^{-3}\text{s}^{-1}$. Other parameters used in computer program implementation are $\gamma = 42666666.67\ \text{s}^{-1}\text{T}^{-1}$ [63], $T_b = 37.0\ ^\circ\text{C}$, $T_m = 1.5\ ^\circ\text{C}$, $M_0 = -500000 \text{Am}^{-1}$, $\xi = 31.6228$, $c_b = 3720 \text{Jkg}^{-1}\text{K}^{-1}$, $t = 3\ \mu\text{s}$ and $\rho_b = 1060 \text{kgm}^{-3}$. The profiles obtained for the brain white matter ($T_1 = 0.78$ s, $T_2 = 0.09$ s [67]) are presented in Fig. 10 while the profiles for controlled neuroprotection of brain white matter ($T_1 = 0.92$ s, $T_2 = 0.10$ s [67]) are presented in Fig. 11.

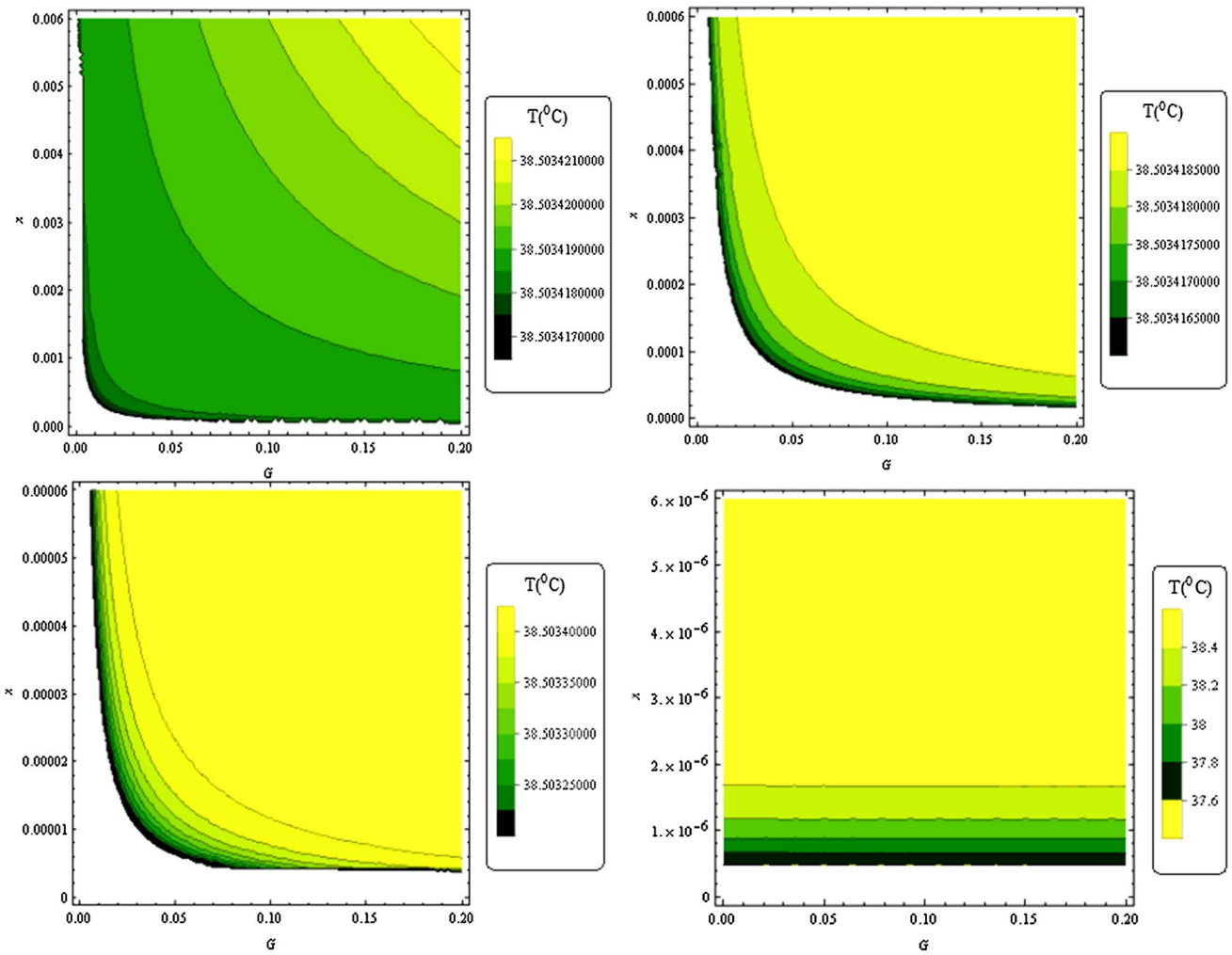

Fig. 5 Contour plots of the derived temperature as a function of the sampling point x and gradient pulse magnitude G for kidney at 1.5T

4 Discussions

We have shown, using the Pennes Bioheat equation and NMR relaxation parameters that it is possible to perform hyperthermia treatment of tumours and monitor temperature changes without the usual concern for safety of normal tissues. At the same time, it has been demonstrated that by modifying the nature of the applied RF field, significant temperature reduction could be induced in order to conduct hypothermia treatment. Appropriate values of SAR have been shown to induce a considerably high thermal response in tumours and very low thermal response towards neuroprotection treatment. It is observed with keen interest that time does not significantly influence the values of the temperature but x does between few millimetres to few micrometre ranges. Consequently, we presented thermal profiles when the sampled regions are within clinical limits.

The thermal profiles in Figs. 1, 2 and 3 were simulated from the computed temperatures in Table 1. The profiles showed the variation of temperature with SAR, volumetric perfusion, thermal conductivity and carefully selected NMR relaxation rates. These rates are unique to different tissues and hence, the ability to be able to represent the relaxation behaviour of different tissues on a thermal profile. This gives us the impressive opportunity to selectively heat tissues with diseases while at the same time monitoring the thermal responses of surrounding normal tissues. The encircled regions on the profiles showed thermal signatures of tumour while the responses of other surrounding tissues were demonstrated as well. This shows that the theranostics approach presented in this study is able to provide real time monitoring of tissues during hyperthermia treatment of tumours so that the surrounding tissues are not overheated in the process.

Figures 4, 5, 6, 7, 8 and 9 were obtained from the Mathematica computer code developed based on Eq. (42) and

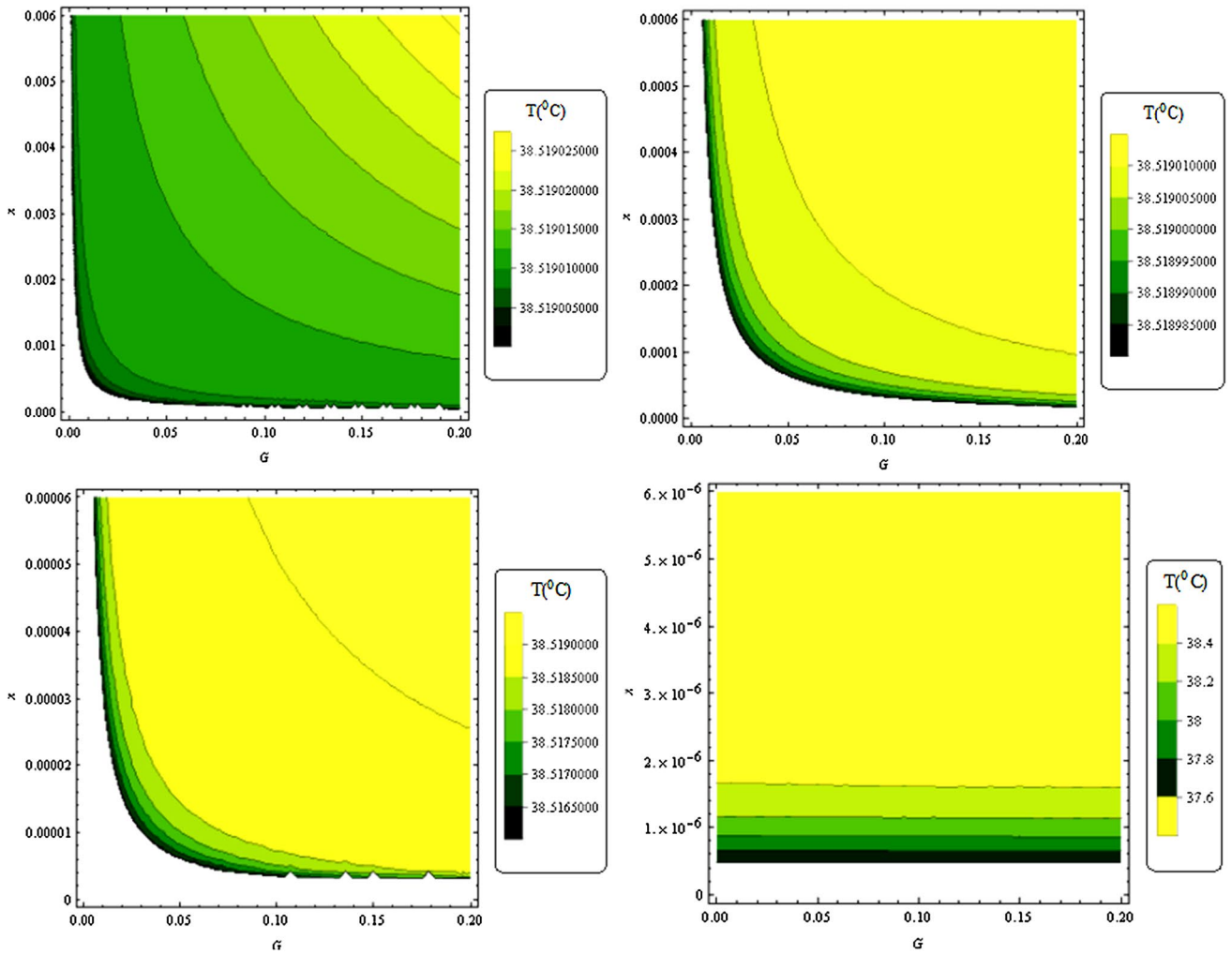

Fig. 6 Contour plots of the derived temperature as a function of the sampling point x and gradient pulse magnitude G for liver at 1.5T

demonstrated the variations of temperature with spatial ranges and gradient field magnitude. The essence of doing this is to find out the amount of gradient field required to achieve hyperthermia in malignant tissues. Fortunately, it is observed that similar amount of gradient field which does not significantly raise the temperatures of different normal tissues (highlighted in Table 1 and shown in Figs. 4, 5, 6, 7 and 8) is able to significantly raise the tumour temperature to hyperthermic limits. We noticed that the unique volumetric perfusion and NMR relaxation times are responsible for this. On a general note, these profiles showed that even with not so significant spatial variations (few micrometers), the thermal contrast is significant and unique for different tissues. Therefore, it has been clearly demonstrated in this study that thermal treatment can be done with the use of NMR properties of tissues for imaging without any fear of RF safety issues. It is noteworthy that the flexibility of the values of the parameter ξ offers quite a lot of interesting possibilities. This is particularly important in regulating the effects of extremely high or low values of the volumetric perfusion. This could also have a relationship to the nature of RF coils used in the theranostics system.

In Figs. 10 and 11, the initial computer code is slightly modified to take into consideration Eqs. (43), (44) and (45) for mapping the thermal responses of both brain white matter and grey matter. This is very important for real time monitoring of hypothermia treatment of problems such as traumatic brain injury, intracerebral hemorrhage and stroke. With these results, we can see the possibility of lowering the temperature in specific areas of the brain to avoid loss of neurons and at the same time monitoring thermal responses of the surrounding tissues so that they are not affected in case the neurons are required for recovery. It is quite interesting to note that despite using the thermal properties of the human brain, the profiles demonstrated that unique NMR relaxation times are able to show impressive contrasts and thermal responses for both white matter and grey matter. The grey matter showed higher thermal responses and the

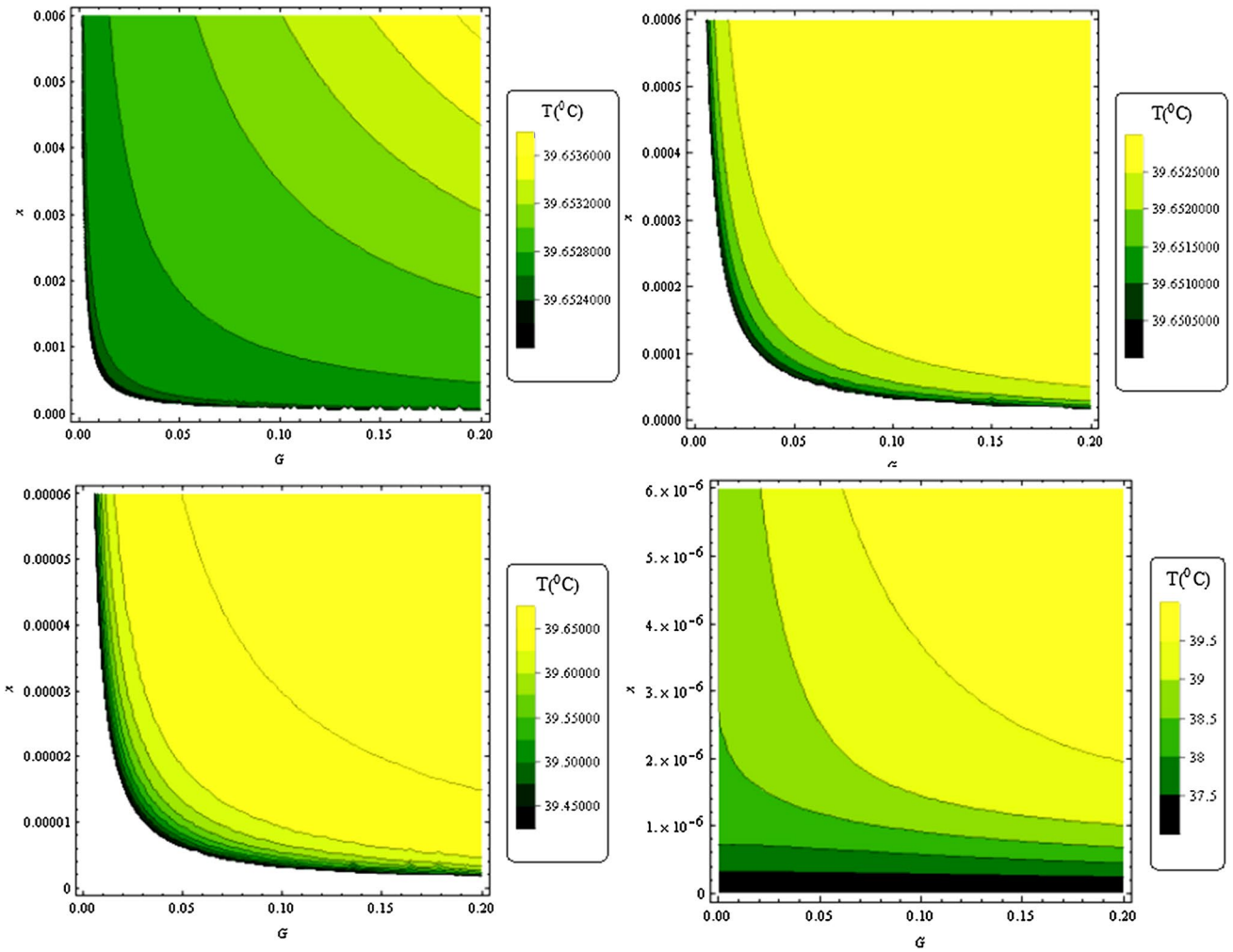

Fig. 7 Contour plots of the derived temperature as a function of the sampling point x and gradient pulse magnitude G for adipose tissue at 1.5T

responses are most significant in the micrometre range. This implies that in order to induce a fast hypothermia response, the region of interest or image voxel should be very small (few microns). Finally, it is worth noticing that the profiles of Figs. 10 and 11 demonstrate the possibility of using the results of this study to detect brain diseases and this could be done during hypothermic treatment as well. This is because diseases significantly influence NMR relaxation times and hence, every small variation in the relaxation times (T_1 and T_2) of brain tissues (which often results in progressive development of diseases) will be imposed on the profiles with unique patterns and thermal responses.

The theranostics method developed in this study is consistent with state-of-the-art in hyperthermia of tumours because their location (x) can now be mapped accordingly (distribution of the relaxation times T_1 and T_2). This is important not only to the tumour location but also (indirectly) to the size of the tumour as demonstrated in Table 1 and Figs. 4, 5, 6, 7, 8, 9, 10 and 11 where measurements of about 5 mm were used. A tumour found in between the reference location and 5 mm is probably much smaller and at early stages of metastasis. The method is able to show sensitive tumour thermal maps at different locations as demonstrated in Fig. 9. Specifically, this method could be used for the assessment of thermal responses at specific tumour depth by choosing the appropriate direction for applying the RF excitation pulse. Considering the symmetry of the human body, the location of tumour from the surface of the body is essentially its depth. Since cancerous cells tend to demonstrate thermal responses that are higher than those of normal tissues, this method is uniquely suited to tumour staging because thermal images presented are responsive to magnetic resonance relaxation times. It is interesting to note that tumour formation, progression and spread have direct influence on NMR relaxation time [68–70] and hence, tumour staging could be imaged with more ease as presented in this investigation.

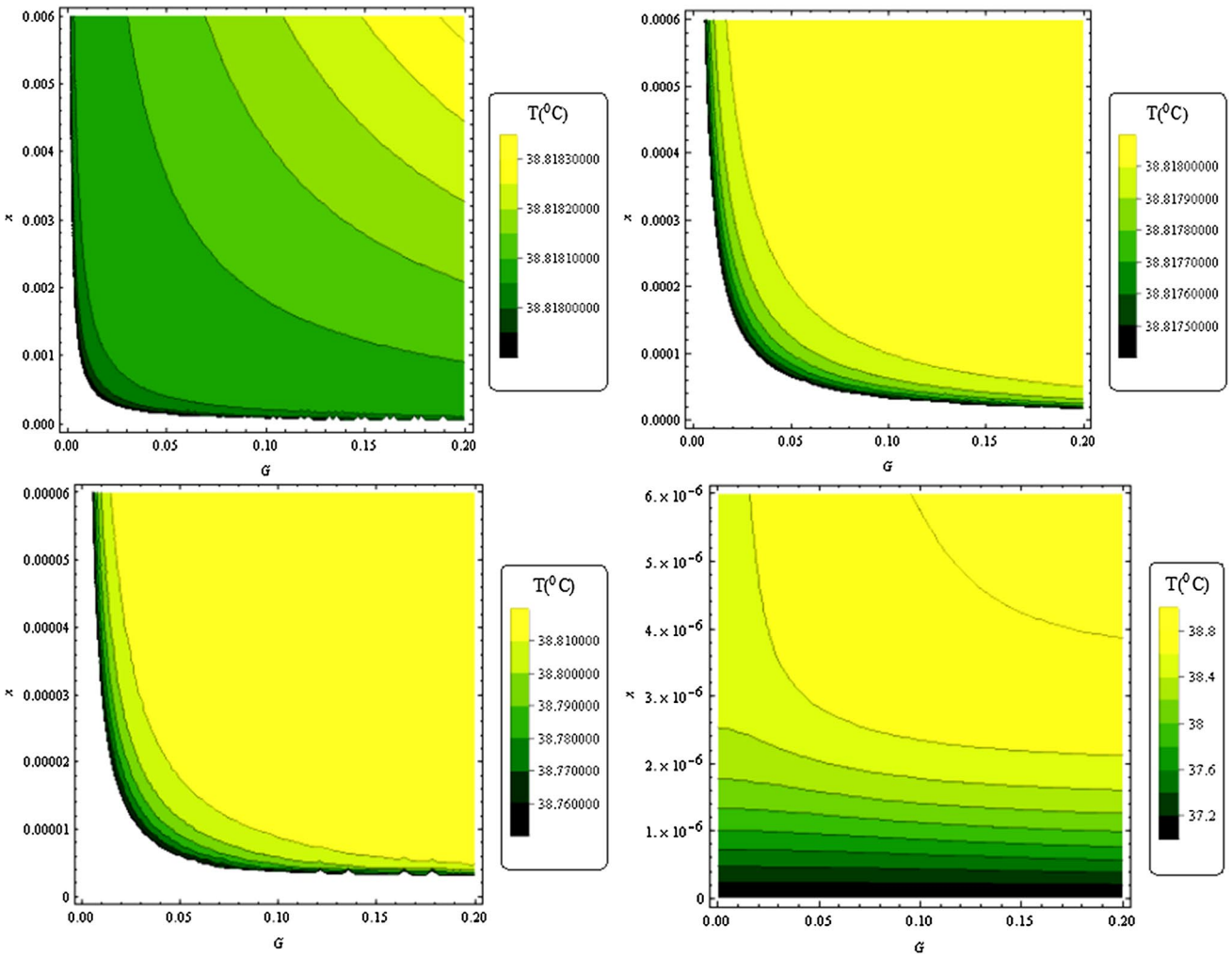

Fig. 8 Contour plots of the derived temperature as a function of the sampling point x and gradient pulse magnitude G for cortical bone at 1.5T

In comparison with other state-of-the-art methods, we have presented a radiofrequency ablation method, which uses a relatively lower frequency (64 MHz) to specifically target only the tumour while keeping the temperature of surrounding normal tissues relatively normal and gives feedback on tissue state via the T_1 and T_2 relaxation times. These features have been demonstrated clearly with the data presented in Table 1. Unlike other methods, which require other clinical techniques to observe tissue response after treatment, our theranostic method could simultaneously treat tumours with thermal deposition while monitoring the tissue response through NMR relaxation times and thermal conductivity (which changes according to tissue state [42, 43, 71, 72]). This feature could be used for local hyperthermia in order to treat superficial, intracavital, intraluminal and intracranial tumours with sizes even smaller than 3 cm. As shown in Fig. 9, the study is able to image tumours whose diameter is as small as 6 μm without the usual fear of side effects of thermal energy deposition in surrounding tissues (as demonstrated in Figs. 4–8), especially when there is an increase in skin temperature. We have also been able to achieve a drastic drop in the length of time for thermal deposition from several minutes to few microseconds (3 μs). This is consistent with the time for heat diffusion in tissues and laser pulse duration during experimental hyperthermia [73].

The problem of limiting target body temperatures when depositing power (SAR) in surrounding tissues have been effectively solved in this study because the model is tissue selective and SAR is now put to a positive use in the models. The control parameters employed and the analytical approach provided the opportunity for better treatment planning towards improved deep regional hyperthermia. For example, as shown in Figs. 1, 2 and 3, the model presented has the capability of computing the tissue target temperature for SAR values and relaxation rates ($1/T_1$ and $1/T_2$) which are not usually allowed because of the limitations placed on hyperthermia machines (with NMR features). This is very important in treatment planning since every possible thermal

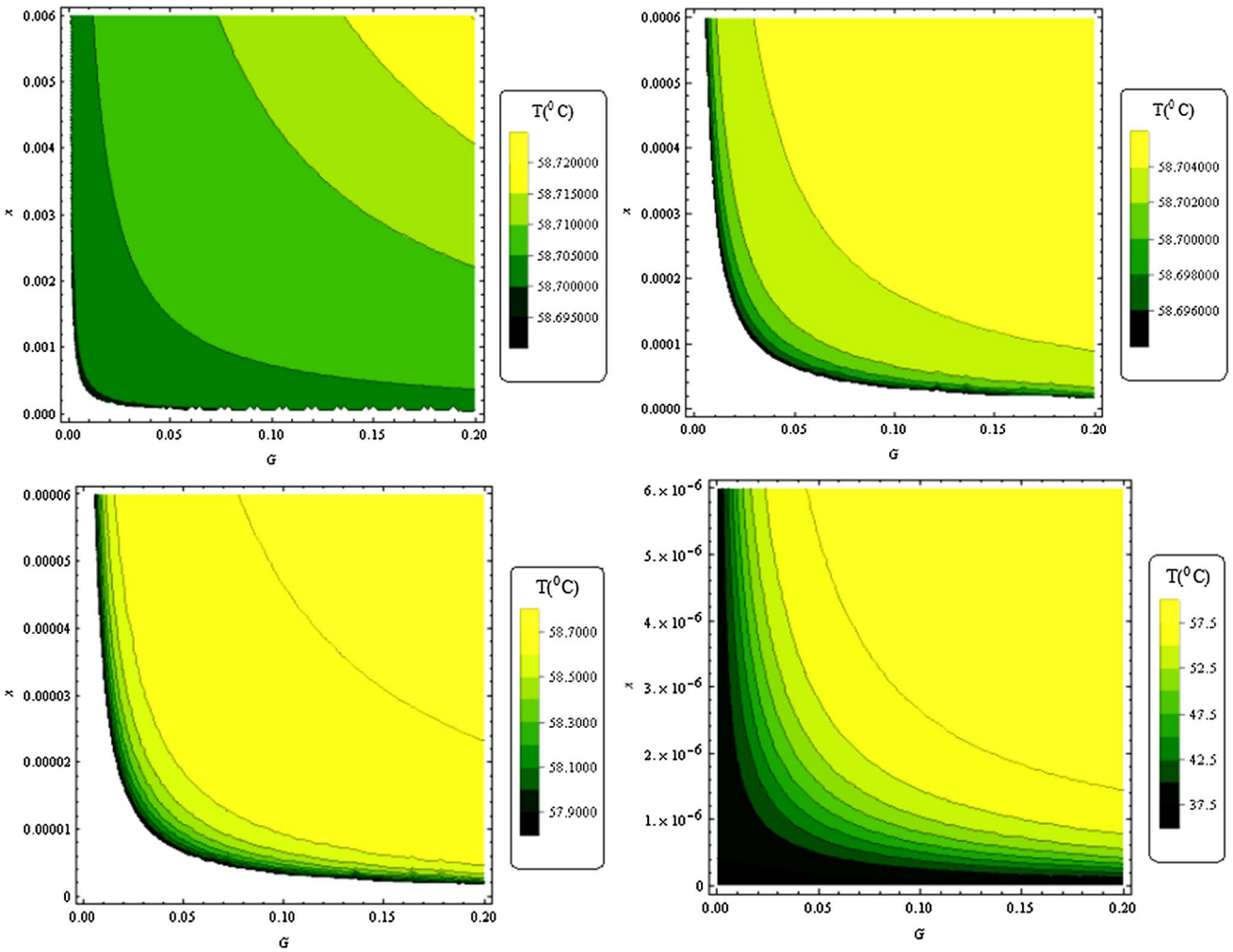

Fig. 9 Contour plots of the derived temperature as a function of the sampling point x and gradient pulse magnitude G for tumor at 1.5T

responses of the target and surrounding tissues could be simulated and envisaged before the actual therapy begins.

The principles of hyperthermia treatment presented in this work are quite straightforward and could translate into the development of portable devices to ensure a homogeneous thermal distribution for whole-body hyperthermia. Since the time to ensure target temperature is drastically reduced in this study, there may be no need for use of sedation and anaesthesia on patients. This feature could also prove to provide a solution to the problem of thermal stress to the heart, liver, lungs or brain.

One of the current challenges of hyperthermia treatment planning, software implementation and integration into the clinical workflow is the uncertainty in dielectric and thermal tissue properties [74], which has constituted hindrance to the simulation accuracy of pre-treatment planning. The analytical approach used in this study does not require the reconstruction of the unknown electric field distribution in the patient and has been able to show the correlation between SAR and tissue temperature. This study has the ability to solve the problem of positioning deviations and allows improvements of mapping treatment planning to thermal dose measurements since we no longer needs a separate system for MRI guidance; our method has incorporated MR guidance into the bio-thermal system. The computer program developed to demonstrate this method is analytical, easy to use and does not require rigorous mathematical skills. The computer program has shown potential in improving target temperature predictions for normal tissues and tumours. This can also prove to be important for bimodality treatment planning since the analytical approach employed could easily be adapted to Eq. (1) to accommodate more source terms (a term including radiotherapy contribution could be included here). As we have pointed out earlier, this could lead to patient-specific treatment plan with better tumour control and minimum risk to surrounding normal tissues.

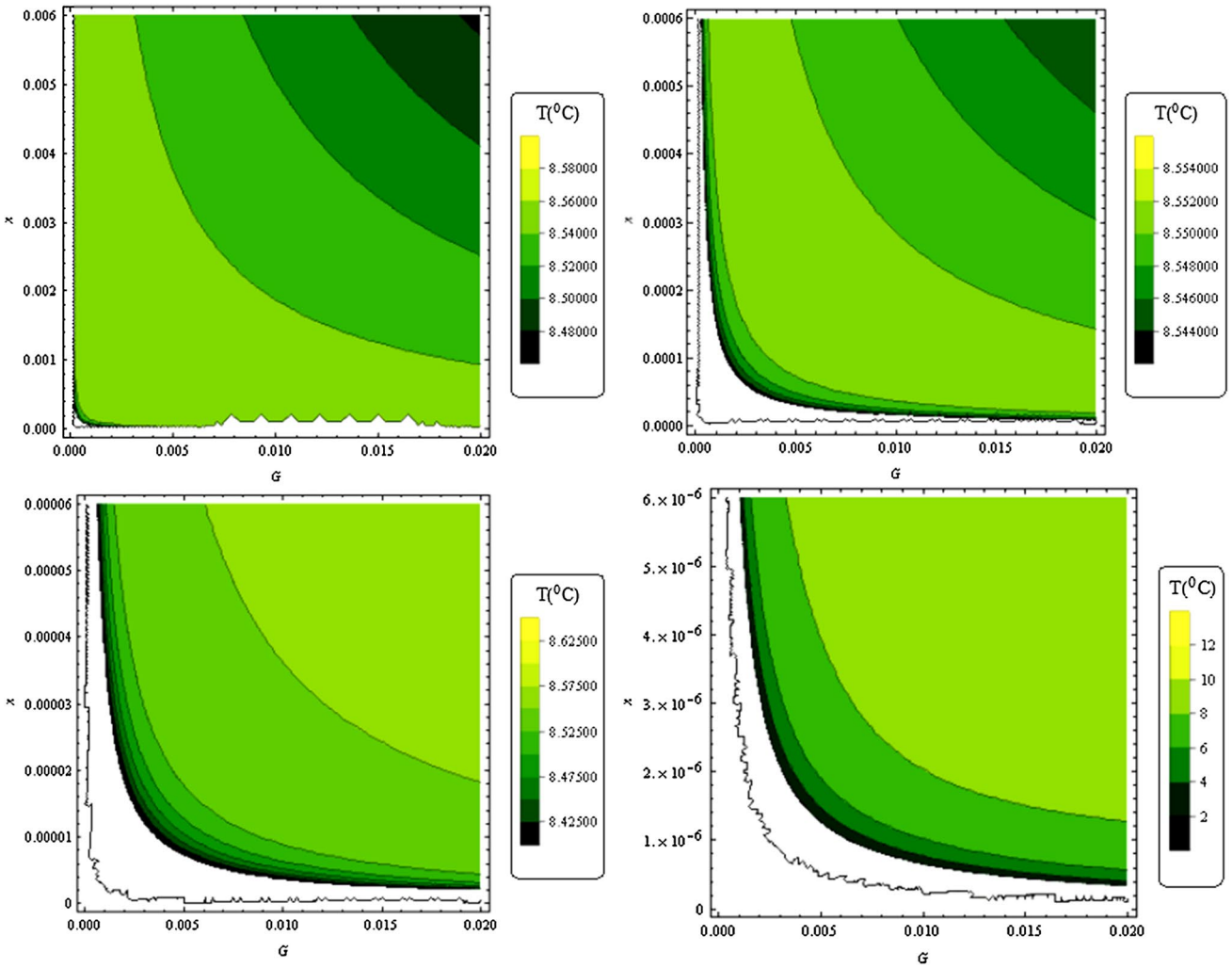

Fig. 10 Contour plots of the derived temperature as a function of the sampling point x and gradient pulse magnitude G for brain white matter at 1.5T

In comparison to most state-of-the-art methods of therapeutic hypothermia, our method has been able to achieve a drastic reduction in the time required to attain the desired tissue temperature from hours and minutes to microseconds (a time of 3 μs has been used in the hypothermia profiles provided in Figs. 10 and 11). This would be helpful in the significant reduction of heat loads on tissues. Secondly, this study uses radiofrequency pulses which rely on tissue spin magnetic resonance and hence, able to penetrate into deep organs. In addition to this, the RF penetration is selective as shown in Figs. 10 and 11 in which thermal profiles of white brain matter and gray brain matter have been provided. We have been able to provide hypothermia treatment to deep organs and do so selectively to components of these organs.

This technique is able to achieve an impressive temperature monitoring and feedback with the incorporation of NMR relaxation times and control parameters such that thermal response monitoring problems associated with current state-of-the-art methods are resolved. This is cheaper to implement for clinical applications. The technique is less cumbersome, not limited to the in-hospital environment and does not have stringent surroundings clean requirements. This is due to its portability and non-invasiveness and could open immense opportunities for use during clinical emergencies.

With the control parameters used in Eqs. (30) and (41), this method could lead to the achievement of optimized cooling within a very short period (microseconds), especially for clinical intra-ischemia cooling. Focal cooling has been reported to have important implications for pathologies of stroke and myocardial infarction [30]. The selectivity as observed in Figs. 10 and 11 allows improved focal cooling in such a way that the temperature of blood flowing to the local tissue environment is not significantly reduced.

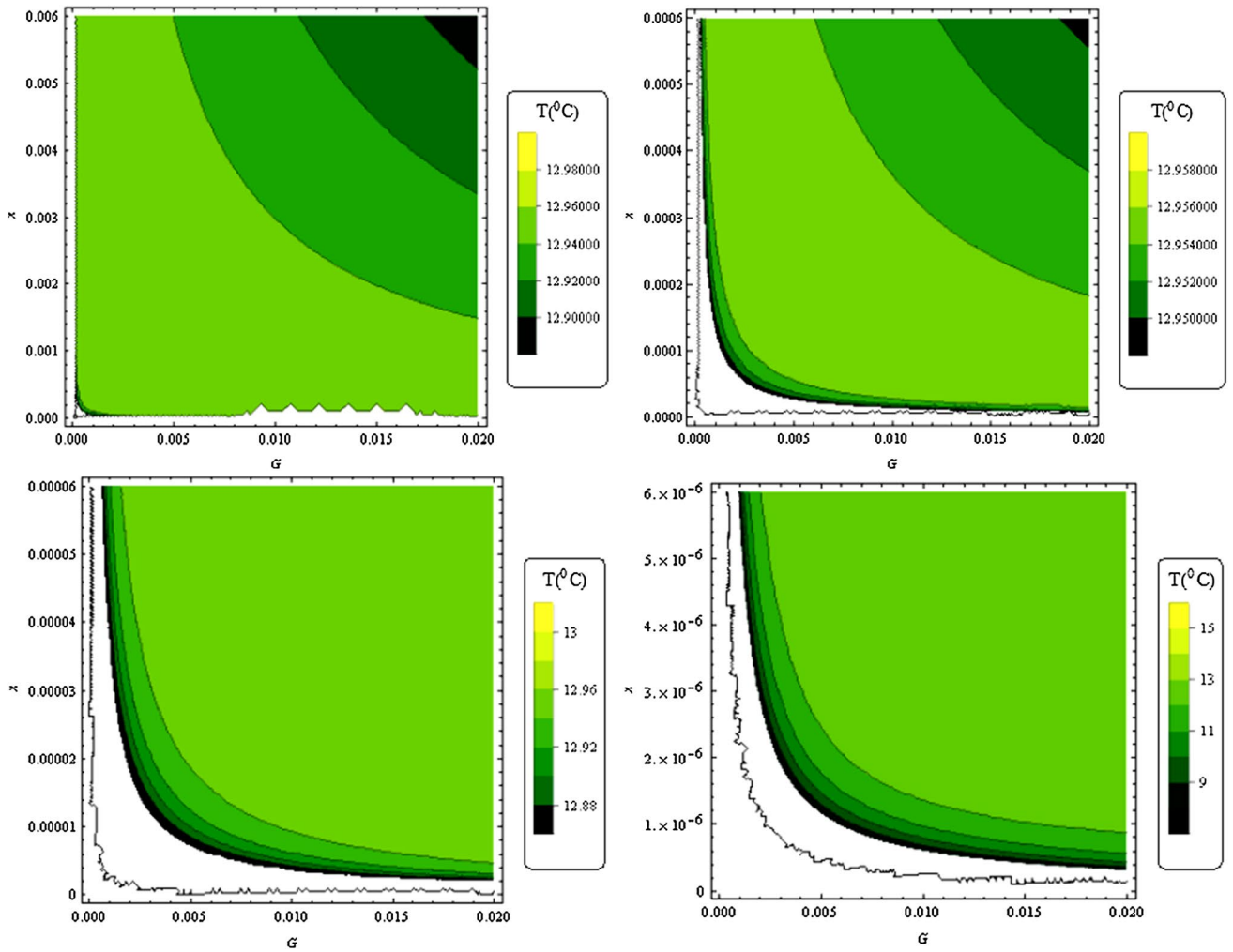

Fig. 11 Contour plots of the derived temperature as a function of the sampling point x and gradient pulse magnitude G for brain grey matter at 1.5T

As stated in the case of hyperthermia of tumours, our method of therapeutic hypothermia appears to have resolved the challenge of temperature monitoring which has placed limitations on the current clinical applications of state-of-the-art methods in therapeutic hypothermia. This has been achieved with the exploration of the unique tissue pathology usually embedded in T_1 and T_2 relaxation times. In fact, the grey brain matter thermal response given in Fig. 11 could help in better monitoring of hippocampal neuron temperature and thermal response of ventricular muscle. The selective thermal deposition feature of our method could prove to be an interesting addition to this monitoring such that the temperatures of ischemic volume centroid can easily be compared during reperfusion as well as rewarming. The diagnostic ability of our method could prove to be helpful in the determination of severity of injury during and after treatment. T_1 and T_2 could help indicate the commencement of ischemia and the nature of the injury. The relaxation times also contain molecular information and hence, they could help in the use of this technique for monitoring cellular events that are affected during ischemia and assessment of protection mechanisms after reperfusion. Finally, it is important to note that this study has opened a window into the future and needs to be explored further for the treatment of patients suffering from cardiac arrest and a few other clinical syndromes that feature ischemic injury. This is also true for patients who are suffering from various types of tumours.

5 Conclusion

We have derived a method that utilizes the principles of magnetic resonance relaxation for the bio-heat transfer phenomenon. An analytical solution to the Pennes bio-heat equation is connected to radiofrequency power absorption in tissues. The solution has been applied to hyperthermia

treatment of tumours and therapeutic hypothermia of the brain. Fortunately, during hyperthermia treatment, the measurement of the actual temperature distribution in the tumour or immediately adjacent tissue is important for the clinical evaluation of the quality of treatment [41], a criterion that is already met in this study.

Several analytical solutions have been provided to Pennes bio-heat equation in which the RF power absorption in the tissues is dependent on the magnetic resonance relaxation parameters. The performance benefits of the new technique are demonstrated through simulations suitable to perform hyperthermia treatment of tumours and monitoring malignant tissue temperature changes without the usual concern for safety of normal tissues. The new theranostics approach can provide real time monitoring of tissues during hyperthermia treatment of tumours so that the surrounding tissues are not overheated in the process.

The model is controlled by relaxation times of tissues and Biothermal features of the tissues. Laboratory realization of this model is not quite difficult because hypothermic and hyperthermic abilities of the model may be combined in a single theranostics modality since the nature of the RF field is responsible for whichever treatment is chosen. Therefore, the design of extremely flexible RF coils is necessary for achieving the gains of this study. Meanwhile, the simulations carried out were done at static magnetic field of 1.5T. It may be informative if the results are checked for higher B_0 fields since RF gradients have different behaviour at these magnetic B_0 fields. This will be the focus of our next investigation. The advantages of this study over the current clinical application of hyperthermia combined with conventional treatment modalities (for example, ionizing radiation, chemotherapy etc.) [75–88] in the treatment of malignant diseases are outlined as follows:

(i) Theranostics approach based on NMR/MRI relaxation parameters is able to provide non invasive real time monitoring of tissues during hyperthermia treatment of tumours such that thermal energy does not induce overheating of normal tissue.
(ii) For damaged brain tissues, it is possible to lower the temperature in specific areas of the brain to avoid loss of neurons and at the same time monitoring thermal responses of the surrounding tissues so that they are not affected in case the neurons are required for recovery.
(iii) Unique NMR relaxation times are able to show impressive contrasts and thermal responses for both white matter and grey matter. This is applicable to other tissues and could be extended to cases where normal and abnormal brain white matter need to be monitored in some neurological diseases such as multiple sclerosis.
(iv) Brain diseases can be detected during hypothermic treatment. This is particularly useful in monitoring of different forms of brain metastasis and the respective disease outcome.
(v) The proposed model can be useful as a control of cancer hyperthermia treatment as well as to control therapeutic hyperthermia through appropriate tuning of RF excitation coils.
(vi) Two controlled parameters were developed to improve the outcome of the new model: ξ as RF dimensionless controlled parameter and $f(x) = T_m$, the constant initial temperature for controlled localized hyperthermia.

It is motivating to note that many parameters of MRI such as the proton density [66, 67], spin–lattice relaxation time (T_1) [75, 76], spin–spin relaxation time (T_2) [77], diffusion coefficient [78, 79], magnetization transfer [80, 81], and proton resonant frequency [75–81], are temperature-dependent and have the potential to be used as temperature indicators. Proton RF as defined in Eqs. (41)–(43) has proved to be superior to other MRI parameters for temperature monitoring of thermal therapies especially because it shows a simple linear correlation with temperature within a relatively large temperature range [83] covering the temperature range of interest for both low-temperature hyperthermia and high-temperature thermal ablation. The computational analysis of Eqs. (41)–(43) and the simulations in Figs. 1, 2, 3, 4, 5, 6, 7 and 8 which give the maximum transient temperature rise in normal tissue as 2 °C (the limit recommended by IEC standard for an MR examination of the torso) makes the new MR thermometry method applicable to moving organs with non-negligible fat content which has been a very challenging goal in international hyperthermia community. Comparably, the same RF energy used for normal tissue produced high temperature levels (11 °C increase) in cancer tissue for hyperthermia therapy subject to T_m and ξ controlled parameters. This may play an increasingly important therapeutic and palliative role as a minimally invasive alternative to surgery.

Acknowledgements We would like to thank Prof. Silvio Aime and Dr. Simona Baroni (both of Chemistry I.F.M. and Molecular Imaging Centre, University of Turin, Turin, Italy) for important lectures which encouraged the idea of this study. The kind suggestions of Prof. Paul R. Stauffer, Director of Thermal Oncology Physics, Thomas Jefferson University, Philadelphia, USA and Prof. Petra H. Kok, Department of Radiation Oncology, Academic Medical Center, Amsterdam who carefully proofread the manuscript as native language speaker are particularly appreciated.

References

1. Rai, P., Mallidi, S., Zheng, X., Rahmanzadeh, R., Mir, Y., Elrington, S., et al. (2010). Development and applications of photo-triggered theranostic agents. *Advanced Drug Delivery Reviews, 62*(11), 1094–1124.
2. Rai, A. J., Yee, J., & Fleisher, M. (2010). Biomarkers in the era of personalized medicine—a multiplexed SNP assay using capillary electrophoresis for assessing drug metabolism capacity. *Scandinavian Journal of Clinical and Laboratory Investigation, 70*(Suppl242), 15–18.
3. Blanchet, K. D. (2010). Redefining personalized medicine in the postgenomic era: developing bladder cancer therapeutics with proteomics. *BJU International, 105,* 1–3.
4. Francke, U. (2010). On the bumpy road towards 'personalized medicine'. *EMBO Molecular Medicine, 2,* 1–2.
5. Bates, S. (2010). Progress towards personalized medicine. *Drug Discovery Today, 15,* 115–120.
6. Espina, V., Liotta, L. A., & Petricoin, E. F. (2009). Reverse-phase protein microarrays for theranostics and patient tailored therapy. *Methods in Molecular Biology, 520,* 89–105.
7. Xiaoyuan, C., & Stephen, W. (2014). Cancer theranostics: an introduction. In C. Xiaoyuan & W. Stephen (Eds.), *Cancer theranostics* (pp. 3–8). Oxford: Academic Press.
8. Kelkar, S. S., & Reineke, T. M. (2011). Theranostics: combining imaging and therapy. *Bioconjugate Chemistry, 22,* 1879–1903.
9. Warenius, H. M. (2009). Technological challenges of theranostics in oncology. *Expert Opinion on Medical Diagnostics, 3,* 381–393.
10. Falk, J. (2008). Epigenetics and sequencing—gene expression systems' second international meeting. Chromatin methylation to disease biology and theranostics. *IDrugs, 11,* 650–652.
11. Lammers, T., Aime, S., Hennink, W. E., Storm, G., & Kiessling, F. (2011). Theranostic nanomedicine. *Accounts of Chemical Research, 44*(10), 1029–1038.
12. Fan, Z., Fu, P. P., Yu, H., & Ray, P. C. (2014). Theranostic nanomedicine for cancer detection and treatment. *Journal of Food and Drug Analysis, 22*(1), 3–17.
13. Alberti, D., Protti, N., Toppino, A., Deagostino, A., Lanzardo, S., Bortolussi, S., et al. (2015). A theranostic approach based on the use of a dual boron/Gd agent to improve the efficacy of Boron Neutron Capture Therapy in the lung cancer treatment. *Nanomedicine: Nanotechnology, Biology and Medicine, 11*(3), 741–750.
14. Bonora, M., Corti, M., Borsa, F., Bortolussi, S., Protti, N., Santoro, D., et al. (2011). ^{1}H and ^{10}B NMR and MRI investigation of boron-and gadolinium–boron compounds in boron neutron capture therapy. *Applied Radiation and Isotopes, 69*(12), 1702–1705.
15. Dada, O. M., Awojoyogbe, O. B., Baroni, S. & Aweda, M.A. (2013). Application of Bloch NMR equation and Pennes bioheat equation to theranostics. In: World molecular imaging society, Annual Congress 2013, Georgia, USA. Late Breaking Abstract Poster Session No. LBAP 055. http://wmis.org/abstracts/2013/data/papers/LBAP055.htm.
16. Habash, R. W., Bansal, R., Krewski, D., & Alhafid, H. T. (2006). Thermal therapy, part 1: an introduction to thermal therapy. *Critical Reviews in Biomedical Engineering, 34*(6), 459.
17. Habash, R. W., Bansal, R., Krewski, D., & Alhafid, H. T. (2006). Thermal therapy, part 2: hyperthermia techniques. *Critical Reviews in Biomedical Engineering, 34*(6), 491.
18. Habash, R. W., Bansal, R., Krewski, D., & Alhafid, H. T. (2007). Thermal therapy, part 3: ablation techniques. *Critical Reviews in Biomedical Engineering, 35*(1–2), 37.
19. Polderman, K. H., Mayer, S. A., & Menon, D. (2008). Hypothermia therapy after traumatic brain injury in children. *New England Journal of Medicine, 359*(11), 1178.
20. Varon, J., Marik, P. E., & Einav, S. (2012). Therapeutic hypothermia: a state-of-the-art emergency medicine perspective. *The American Journal of Emergency Medicine, 30*(5), 800–810.
21. Alzaga, A. G., Cerdan, M., & Varon, J. (2006). Therapeutic hypothermia. *Resuscitation, 70*(3), 369–380.
22. Varon, J., & Acosta, P. (2008). Therapeutic hypothermia: past, present, and future. *Chest Journal, 133*(5), 1267–1274.
23. Rincon, F., & Mayer, S. A. (2006). Therapeutic hypothermia for brain injury after cardiac arrest. In: *Seminars in neurology* (Vol. 26, No. 04, pp. 387–395). Copyright© 2006 by Thieme Medical Publishers, Inc., 333 Seventh Avenue, New York, NY 10001, USA.
24. Varon, J., & Marik, P. E. (2006). Complete neurological recovery following delayed initiation of hypothermia in a victim of warm water near-drowning. *Resuscitation, 68*(3), 421–423.
25. Baena, R. C., Busto, R., Dietrich, W. D., Globus, M. T., & Ginsberg, M. D. (1997). Hyperthermia delayed by 24 h aggravates neuronal damage in rat hippocampus following global ischemia. *Neurology, 48*(3), 768–773.
26. O'sullivan, S. T., O'shaughnessy, M., & O'connor, T. P. F. (1995). Baron Larrey and cold injury during the campaigns of Napoleon. *Annals of Plastic Surgery, 34*(4), 446–449.
27. Nolan, J. P., Morley, P. T., Hoek, T. V., Hickey, R. W., Kloeck, W. G. J., Billi, J., et al. (2003). Therapeutic hypothermia after cardiac arrest. *Circulation, 108*(1), 118–121.
28. Nolan, J. P., Morley, P. T., Hoek, T. L., Hickey, R. W., & Advancement Life support Task Force of the International Liaison committee on Resuscitation. (2003). Therapeutic hypothermia after cardiac arrest: An advisory statement by the Advancement Life Support Task Force of the International Liaison Committee on Resuscitation. *Resuscitation, 57,* 231–235.
29. Haugk, M., Sterz, F., Grassberger, M., Uray, T., Kliegel, A., Janata, A., et al. (2007). Feasibility and efficacy of a new non-invasive surface cooling device in post-resuscitation intensive care medicine. *Resuscitation, 75*(1), 76–81.
30. Lampe, J. W., & Becker, L. B. (2011). State of the art in therapeutic hypothermia. *Annual Review of Medicine, 62,* 79–93.
31. Marshall, L. F. (2000). Head injury: recent past, present, and future. *Neurosurgery, 47*(3), 546–561.
32. Chicheł, A., Skowronek, J., Kubaszewska, M., & Kanikowski, M. (2007). Hyperthermia description of a method and a review of clinical applications. *Reports of Practical Oncology & Radiotherapy, 12*(5), 267–275.
33. Sneed, P. K., Stauffer, P. R., Li, G. C., Stege, G. J. J. (2004). Hyperthermia. In: Leibel S. A., Phillips T. L. (Eds.), *Textbook of radiation oncology*, 2nd ed. Chapter 70 (pp. 1569–1596). Saunders.
34. Van der Zee, J. (2002). Heating the patient: a promising approach? *Annals of Oncology, 13*(8), 1173–1184.
35. Stauffer, P. R., & Goldberg, S. N. (2004). Introduction: thermal ablation therapy. *International Journal of Hyperthermia, 20*(7), 671–677.
36. Carter, D. L., MacFall, J. R., Clegg, S. T., Wan, X., Prescott, D. M., Charles, H. C., et al. (1998). Magnetic resonance thermometry during hyperthermia for human high-grade sarcoma. *International Journal of Radiation Oncology, Biology, Physics, 40*(4), 815–822.
37. Wust, P., Hildebrandt, B., Sreenivasa, G., Rau, B., Gellermann, J., Riess, H., et al. (2002). Hyperthermia in combined treatment of cancer. *The lancet Oncology, 3*(8), 487–497.
38. Hanusch, K. U., Janssen, C. H., Billheimer, D., Jenkins, I., Spurgeon, E., Lowry, C. A., et al. (2013). Whole-body hyperthermia for the treatment of major depression: associations with thermoregulatory cooling. *American Journal of Psychiatry, 170*(7), 802–804.

39. Jha, S., Sharma, P. K., & Malviya, R. (2016). Hyperthermia: role and risk factor for cancer treatment. *Achievements in the Life Sciences, 10*(2), 161–167.
40. Alexander, H. R. (2001). Isolation perfusion. In V. T. DeVita, S. Hellman, & S. A. Rosenberg (Eds.), *Cancer: principles and practice of oncology* (6th ed., Vol. 1–2, pp. 1–2). Philadelphia: Lippincott Williams and Wilkins.
41. Falk, M. H., & Issels, R. D. (2001). Hyperthermia in oncology. *International Journal of Hyperthermia, 17*(1), 1–18.
42. Brix, G., Seebass, M., Hellwig, G., & Griebel, J. (2002). Estimation of heat transfer and temperature rise in partial-body regions during MR procedures: an analytical approach with respect to safety considerations. *Magnetic Resonance Imaging, 20,* 65–76.
43. Tzu-Ching, S., Ping, Y., Win-Li, L., & Hong-Sen, K. (2007). Analytical analysis of the Pennes bioheat transfer equation with sinusoidal heat flux condition on skin surface. *Medical Engineering and Physics, 29,* 946–953.
44. Chopra, R., Wachsmuth, J., Burtnyk, M., Haider, M. A., & Bronskill, M. J. (2006). Analysis of factors important for transurethral ultrasound prostate heating using MR temperature feedback. *Physics in Medicine and Biology, 51,* 827–844.
45. Jiang, S. C., Ma, N., Li, H. J., & Zhang, X. X. (2002). Effects of thermal properties and geometrical dimensions on skin burn injuries. *Burns, 28,* 713–717.
46. Ng, E. Y. K., & Chua, L. T. (2002). Comparison of one- and two-dimensional programmes for predicting the state of skin burns. *Burns, 28,* 27–34.
47. Chen, C., & Xu, L. X. (2002). Tissue temperature oscillations in an isolated pig kidney during surface heating. *Annals of Biomedical Engineering, 30,* 1162–1171.
48. Liu, E. H., Saidel, G. M., & Harasaki, H. (2003). Model analysis of tissue responses to transient and chronic heating. *Annals of Biomedical Engineering, 31,* 1007–1048.
49. Spiegel, M. R. (1983). *Schaum's Outline series of theory and problems of advanced mathematics for engineers and scientists*. Singapore: McGraw-Hill.
50. Tabatabaei, S., Zhao, T., Awojoyogbe, O., & Moses, F. (2009). Cut-off cooling velocity profiling inside a keyhole model using the Boubaker polynomials expansion scheme. *Heat Mass Transfer, 45,* 1247–1251.
51. Aweda, M. A., Agida, M., Dada, M., Awojoyogbe, O. B., Isah, K., & Faromika, O. P. (2011). A solution to laser-induced heat equation inside a two-layer tissue model using boubaker polynomials expansion scheme. *Journal of Laser Micro/Nanoengineering, 6*(2), 105–109.
52. Dada, M., Awojoyogbe, O. B., & Boubaker, K. (2011). Temperature profiling during the extinction phase of laser keyhole welding using the Boubaker polynomials expansion scheme (BPES). *Optics and Laser Technology, 43*(3), 546–549.
53. Abragam, A. (1961). *The principles of nuclear magnetism*. Oxford: Clarendon Press.
54. Brix, G., Kolem, H., Nitz, W. R., Bock, M., Huppertz, A., Zech, C. J., et al. (2008). *Basics of MRI and MRS*. Berlin: Springer.
55. Laurent, S., Forge, D., Port, M., Roch, A., Robic, C., Elst, L. V., et al. (2008). Magnetic iron oxide nanoparticles: synthesis, stabilization, vectorization, physicochemical characterizations, and biological applications. *Chemical Reviews, 108,* 2064–2110.
56. Cowan, B. P. (1997). *Nuclear magnetic resonance and relaxation* (1st ed.). Cambridge: Cambridge University Press.
57. Slichter, C. P. (1963). *Principles of magnetic resonance*. New York: Harper and Row.
58. Dada, O. M., Awojoyogbe, O. B., Adesola, O. A., & Boubaker, K. (2013). Magnetic resonance imaging-derived flow parameters for the analysis of cardiovascular diseases and drug development. *Magnetic Resonance Insights, 6,* 83–93.
59. Gupta, A., Stait-Gardner, T., Ghadirian, B., Price, W. S., Dada, O. M., & Awojoyogbe, O. B. (2014). *Theory, dynamics and applications of magnetic resonance imaging-I*. New York: Science Publishing Group.
60. Awojoyogbe, O. B., Dada, O. M., Onwu, O. S., Ige, A. T., & Akinwande, I. N. (2016). Computational diffusion magnetic resonance imaging based on time-dependent bloch nmr flow equation and bessel functions. *Journal of Medical Systems, 40,* 106.
61. Dada, M. O., Jayeoba, B., Awojoyogbe, B. O., Uno, U. E., & Awe, O. E. (2017). Mathematical development and computational analysis of harmonic phase-magnetic resonance imaging (HARP-MRI) based on bloch nuclear magnetic resonance (NMR) diffusion model for myocardial motion. *Journal of Medical Systems, 41*(10), 168.
62. Moroz, P., Jones, S. K., & Gray, B. N. (2001). Status of hyperthermia in the treatment of advanced liver cancer. *Journal of Surgical Oncology, 77*(4), 259.
63. Price, W. S. (1997). Pulsed field gradient nuclear magnetic resonance as a tool for studying translational diffusion: part I. Basic theory. *Concepts in Magnetic Resonance, 9,* 299–336.
64. Wartenberg, K. A., & Mayer, S. A. (2008). Use of induced hypothermia for neuroprotection: indications and applications. *Future Neurology, 3*(3), 325–361.
65. Wagner, K. R., & Zuccarello, M. (2005). Local brain hypothermia for neuroprotection in stroke treatment and aneurysm repair. *Neurological Research, 27*(3), 238–245.
66. Awojoyogbe, O. B., & Dada, M. (2013). Mathematical design of a magnetic resonance imaging sequence based on Bloch NMR flow equations and Bessel functions. *Chinese Journal of Magnetic Resonance Imaging, 5,* 373–381.
67. Moratal, D., Brummer, M. E., Martí-Bonmatí, L., & Vallés-Lluch, A. (2006). NMR Imaging. In: *Wiley encyclopedia of biomedical engineering*.
68. Deoni, S. C. (2010). Quantitative relaxometry of the brain. *Topics in Magnetic Resonance Imaging, 21*(2), 101.
69. Wagner-Manslau, C., Lukas, P., Herzog, M., Kau, R., & Beckers, K. (1994). MRI and proton-NMR relaxation times in diagnosis and therapeutic monitoring of squamous cell carcinoma. *European Radiology, 4*(4), 314–323.
70. Chatell, M., Darcel, F., de Certaines, J., Benoist, L., & Bernard, A. M. (1986). T1 and T2 proton nuclear magnetic resonance (NMR) relaxation times in vitro and human intracranial tumours. *Journal of Neuro-Oncology, 3*(4), 315–321.
71. Bhattacharya, A., & Mahajan, R. L. (2003). Temperature dependence of thermal conductivity of biological tissues. *Physiological Measurement, 24*(3), 769.
72. Rossmann, C., & Haemmerich, D. (2014). Review of temperature dependence of thermal properties, dielectric properties, and perfusion of biological tissues at hyperthermic and ablation temperatures. *Critical Reviews™ BioMedical Engineering, 42*(6), 467.
73. Ansari, M. A., Erfanzadeh, M., & Mohajerani, E. (2013). Mechanisms of laser-tissue interaction: II. Tissue thermal properties. *Journal of lasers in medical sciences, 4*(3), 99.
74. Kok, H. P., Wust, P., Stauffer, P. R., Bardati, F., Van Rhoon, G. C., & Crezee, J. (2015). Current state of the art of regional hyperthermia treatment planning: a review. *Radiation Oncology, 10*(1), 196.
75. Chen, J., Daniel, B. L., & Pauly, K. B. (2006). Investigation of proton density for measuring tissue temperature. *Journal of Magnetic Resonance Imaging, 23,* 430–434.
76. Gultekin, D. H., & Gore, J. C. (2005). Temperature dependence of nuclear magnetization and relaxation. *Journal of Magnetic Resonance, 172,* 133–141.
77. Parker, D. L., Smith, V., Sheldon, P., Crooks, L. E., & Fussell, L. (1983). Temperature distribution measurements in two-dimensional NMR imaging. *Medical Physics, 10*(3), 321–325.

78. Bottomley, P. A., Foster, T. H., Argersinger, R. E., & Pfeifer, L. M. (1984). A review of normal tissue hydrogen NMR relaxation times and relaxation mechanisms from 1 to 100 MHz: dependence on tissue type, NMR frequency, temperature, species, excision, and age. *Medical Physics, 11*(4), 425–448.
79. Graham, S. J., Bronskill, M. J., & Henkelman, R. M. (1998). Time and temperature dependence of MR parameters during thermal coagulation of ex vivo rabbit muscle. *Magnetic Resonance in Medicine, 39,* 198–203.
80. Le Bihan, D., Delannoy, J., & Levin, R. L. (1989). Temperature mapping with MR imaging of molecular diffusion: application to hyperthermia. *Radiology, 171,* 853–857.
81. Bleier, A. R., Jolesz, F. A., Cohen, M. S., Weisskoff, R. M., Dalcanton, J. J., Higuchi, N., et al. (1991). Real-time magnetic resonance imaging of laser heat deposition in tissue. *Magnetic Resonance in Medicine, 21,* 132–137.
82. Young, I. R., Hand, J. W., Oatridge, A., & Prior, M. V. (1994). Modeling and observation of temperature changes in vivo using MRI. *Magnetic Resonance in Medicine, 32*(3), 358–369.
83. Graham, S. J., Stanisz, G. J., Kecojevic, A., Bronskill, M. J., & Henkelman, R. M. (1999). Analysis of changes in MR properties of tissues after heat treatment. *Magnetic Resonance in Medicine, 42*(6), 1061–1071.
84. Hindman, J. C. (1966). Proton resonance shift of water in the gas and liquid states. *The Journal of Chemical Physics, 44*(12), 4582–4592.
85. Ishihara, Y., Calderon, A., Watanabe, H., et al. (1995). A precise and fast temperature mapping using water proton chemical shift. *Magnetic Resonance in Medicine, 34,* 814–823.
86. De Poorter, J. (1995). Noninvasive MRI thermometry with the proton resonance frequency method: study of susceptibility effects. *Magnetic Resonance in Medicine, 34,* 359–367.
87. Poorter, J. D., Wagter, C. D., Deene, Y. D., Thomsen, C., Ståhlberg, F., & Achten, E. (1995). Noninvasive MRI thermometry with the proton resonance frequency (PRF) method: in vivo results in human muscle. *Magnetic Resonance in Medicine, 33*(1), 74–81.
88. Kuroda, K. (2005). Non-invasive MR thermography using the water proton chemical shift. *International Journal of Hyperthermia, 21,* 547–560.